ELSEVIER

Biophysical Chemistry 117 (2005) 119 – 140

Biophysical Chemistry

http://www.elsevier.com/locate/biophyschem

Structures and stability of salt-bridge in aqueous solution

Kritsana Sagarik[a,*], Supaporn Chaiyapongs[b]

[a]School of Chemistry, Institute of Science, Suranaree University of Technology, Nakhon Ratchasima 30000, Thailand
[b]Department of Chemistry, Faculty of Science, Ramkhamhaeng University, Bangkok 10240, Thailand

Received 16 February 2005; accepted 21 April 2005
Available online 1 June 2005

Abstract

Structures and stability of salt-bridges in aqueous solutions were investigated using a complex formed from the guanidinium (Gdm^+) and formate (FmO^-) ions as a model system. The Test-particle model (T-model) potentials to describe the interactions in the Gdm^+–H_2O, FmO^-–H_2O and Gdm^+–FmO^- complexes were constructed, tested and applied in molecular dynamics (MD) simulations of the aqueous solutions at 298 K. The three-dimensional structures and energetic of the hydrogen bond (H-bond) networks of water in the first hydration shells of the Gdm^+ and FmO^- ions, as well as the Gdm^+–FmO^- complex, were visualized and analyzed using various probability distribution (PD) maps. The structures of the average potential energy landscapes at the H-bond networks were employed to characterize the stability and dynamic behavior of water molecules in the first hydration shells of the solutes. It was observed that water molecules in the first hydration shell of the close-contact Gdm^+–FmO^- complex form associated H-bond networks, which introduce a net stabilization effect to the ion-pair, whereas those in the interstitial H-bond network destabilize and break the solvent-separated Gdm^+–FmO^- complex. The present results showed that, in order to provide complete insights into the structures and stability of ion-pairs in aqueous solutions, explicit water molecules have to be included in the model calculations.

Keywords: Guanidinium; Formate; Salt-bridge; Ion-pair; Hydration

1. Introduction

Salt-bridges or ion-pairs have been of interest since, on average, one-third of the charged residues in proteins are involved in ion-pairs, and about 76% of these play important roles in stabilization of the protein secondary and tertiary structures [1,2]. Due to strong electrostatic interaction, salt-bridges have also been recognized to possess other specific functions to perform, especially in globular proteins [2]. They were suggested, for example, to act as active mediator for molecular recognition in enzymes and proteins [3–5]. About 40% of ion-pairs within proteins involve arginine–carboxylate (Arg–COO^-) interactions [2,6], e.g., the arginine–glutamate (Arg–Glu) and arginine–aspartate (Arg–Asp) side-chain interactions. Therefore, the guanidinium (Gdm^+) and formate (FmO^-) ions [7,8], as well as the methylguanidinium ($MGdm^+$) and acetate (AcO^-) ions [9,10], have been frequently chosen as model systems in the studies of ion-pair interactions between side-chains of proteins. It was pointed out based on 37 high-resolution protein structures that the most preferential structure for the Arg–COO^- interaction is represented by a planar structure, in which a single N–H···O–C hydrogen bond (H-bond) is the most common type of interaction; whereas double N–H···O–C H-bonds are also frequently found [6]. By extracting orientation information from protein coordinate data, in comparison with the results of electrostatic modeling of the $MGdm^+$–AcO^- complex, the authors in Ref. [11] concluded that, due to the electrostatic domination, the so-called "side-on" and "end-on" doubly N–H···O–C H–bond configurations are the most favorable, with the side-on being slightly lower in energy. Additionally, the analysis of protein crystal structure data

* Corresponding author. Tel./fax: +66 44 224 635.
E-mail address: kritsana@ccs.sut.ac.th (K. Sagarik).

0301-4622/$ - see front matter © 2005 Elsevier B.V. All rights reserved.
doi:10.1016/j.bpc.2005.04.012

[11] showed that the end-on structure is more preferential for the intermolecular interactions and the side-on for the intramolecular ones. According to a systematic geometric analysis of the Brookhaven Protein Data Bank (PDB), the stereochemistry of the side-chain H-bonds of proteins was pointed out to be characterized by at least three factors: (a) the electronic configuration of the H-bond acceptor atoms; (b) the steric accessibility of the H-bond donor atoms and; (c) the conformation of amino acid side-chains [12].

Several theoretical investigations were made on model salt-bridges in the gas phase, aqueous and non-aqueous solutions, using both continuum [8,9] and explicit solvent models [13,14]. When a continuum model with the self-consistent reaction field (SCRF) method was applied in the investigation of the $MGdm^+-AcO^-$ complex in aqueous solutions ($[MGdm^+-AcO^-]_{aq}$) [9], the solvent induced destabilization of the salt-bridge interaction was observed. It was also illustrated that the preference of the ion-pairs over the neutral complexes in polar solvents is considerably reduced or even reversed in very low dielectric media, such as chloroform [9] and CCl_4 [8]. The authors in Ref. [9] stressed the effects of environment on the H-bonds in the ion-pairs. Through an explicit water model, molecular dynamics (MD) free energy calculations were performed on $[MGdm^+-AcO^-]_{aq}$, using various approaches to take into account long-range electrostatic interaction [14]. The potential of mean force (PMF) for the doubly N–H···O–C H-bond configuration showed minima which are the characteristic of both close-contact and solvent-separated ion-pairs [14]. However, the free energy profiles of the Gdm^+-AcO^- and methylammonium–AcO^- (MAm^+-AcO^-) complexes, computed from Monte Carlo (MC) simulations, displayed only a single shallow free energy minimum at the distance corresponding to the close-contact ion-pairs [13]. The shallow free energy minimum suggested that the association between the ions in aqueous solutions is not particularly strong. The authors in Ref. [13] described the existence of double minima on the free energy profile as a result of the constraint imposed on the relative orientation of the ions in the PMF calculations.

Although in principle, ab initio calculations with continuum model such as the SCRF method could provide useful information on molecular association in continuum solvent characterized by a dielectric constant, more and more theoretical and experimental evidences showed the necessity to include the details of solvent molecules in model calculations, especially for H-bond systems [15]. This is due to the fact that continuum models neglect specific short-range solute–solvent interaction, as well as the behavior and structures of solvent molecules in the first solvation shell of solute. Continuum models were pointed out to be suitable only for the systems, in which solvents act only as perturbation on the gas-phase property of the system [15].

According to the literature survey, at least four remarks could be made in the field of salt-bridge interactions in solutions: (a) previous theoretical and experimental investigations tend to focus attention only on the effects of solute–solute and solute–solvent interactions; (b) the detail information on the solvent structures especially in the first solvation shell of solute has been neglected in many investigations; (c) due to the limitation of computer resources, there has been an increasing number of theoretical studies made based on continuum models; (d) there were few theoretical and experimental investigations which combine structural and energetic effects, as well as the dynamic behavior of solvent molecules in the first solvation shell of solute, in the study of ion-pairs in solutions, etc. These remarks partly formed the basis of our previous theoretical investigations on alanine zwitterion in aqueous solutions ($[Alaz]_{aq}$) [16], in which the detail structures and energetic of the H-bond networks of water in the first hydration shell of Alaz were derived from MD simulations. In Ref. [16], the three-dimensional structures of the H-bond networks of water were analyzed and visualized using various probability distribution (PD) maps, such as the oxygen (PDO) and hydrogen probability distribution (PDH) maps, as well as the average solute–solvent (AWPD) and solvent–solvent interaction energy probability distribution (WWPD) maps. The structures of the average potential energy landscapes were employed to describe the dynamic behavior of water molecules in the first hydration shell of the functional groups of Alaz. They were computed from the total-average interaction energy probability distribution (AW-WWPD) maps. The probabilities for the water exchange, both within the H-bond networks and between the H-bond networks and the outsides, were anticipated from these pieces of information. It was concluded in Ref. [16] that a complete picture of molecular hydration could be obtained only when explicit water molecules, together with their hydration dynamics in the first hydration shell, are considered in the model calculations.

In the present work, the structures and energetic of a model salt-bridge formed from Gdm^+ and FmO^- were studied, both in the gas phase and aqueous solutions. The present theoretical investigation started with construction of intermolecular potentials to describe the interactions in the Gdm^+-H_2O, FmO^--H_2O and Gdm^+-FmO^- complexes, using the Test-particle model (T-model) [17–20]. The T-model potentials were applied in the calculations of the equilibrium structures and interaction energies of the Gdm^+-H_2O, FmO^--H_2O and Gdm^+-FmO^- complexes in the gas phase. Some lowest-lying minimum energy geometries of these H-bond complexes were tested using ab initio calculations at the MP2 level of theory. The computed T-model potentials were applied in MD simulations of $[Gdm^+]_{aq}$, $[FmO^-]_{aq}$ and $[Gdm^+-FmO^-]_{aq}$ at 298 K. In order to obtain information on the three-dimensional structures and the stability of the H-bond networks in the first hydration shells of solutes, the MD results were

visualized and analyzed using the PDO, AWPD and AWWWPD maps, as described in Ref. [21]. The average potential energy landscapes and the H-bond lifetimes were used to characterize the dynamic behavior of water molecules in the first hydration shells of solutes. The results were discussed in comparison with available theoretical and experimental results of the same and similar systems.

2. Methods

2.1. The T-model potentials

The derivation and application of the T-model on various chemical systems have been presented in details elsewhere [16–20,22–30]. Here, only some important aspects of the T-model are briefly summarized. In the present work, the optimized geometries of the Gdm^+ and FmO^- ions were obtained from ab initio calculations at MP2/6-311++G(d,p) and MP2/6-311++G(3df,3pd) levels of theory, respectively. They were kept constant throughout the calculations.

Within the framework of the T-model, the interaction energy ($\Delta E_{\text{T-model}}$) between molecules A and B is written as a sum of the first-order interaction energy (ΔE^1_{SCF}) and a higher-order energy term (ΔE^r).

$$\Delta E_{\text{T-model}} = \Delta E^1_{\text{SCF}} + \Delta E^r \tag{1}$$

ΔE^1_{SCF} accounts for the exchange repulsion and electrostatic energies. It is computed from ab initio SCF calculations and takes the following analytical form:

$$\Delta E^1_{\text{SCF}} = \sum_{i\epsilon A}\sum_{j\epsilon B}\left[\exp\left(\frac{-R_{ij}+\sigma_i+\sigma_j}{\rho_i+\rho_j}\right)+\frac{q_iq_j}{R_{ij}}\right] \tag{2}$$

i and j in Eq. (2) label the sites of molecules A and B. σ_i, ρ_i and q_i are the site parameters. R_{ij} is the site–site distance. The exponential term in Eq. (2) relates to the size and shape of interacting molecules A and B. The point charges, q_i and q_j, are computed from the requirement that a point-charge model reproduces the electrostatic potentials of molecule of interest. In our previous studies [16,28–30], it was shown that the CHelpG charges [31] are also applicable and quite practical. Therefore, in the present work, the point charges for Gdm^+ and FmO^- were determined by a fit of the electrostatic potentials at points selected according to the CHelpG scheme, using GAUSSIAN 98 [32]. For the Gdm^+ and FmO^- ions, the electrostatic potentials employed in the fit were computed from ab initio calculations at the HF/6-311++G(d,p) and HF/6-311++G(3df,3pd) levels of theory, respectively. Due to the symmetry, the dipole moment for Gdm^+ is 0 D; whereas that for FmO^- is 1.90 D, which is in good agreement with those reported in Ref. [33] between 1.6 to 1.7 D.

ΔE^r in Eq. (1) represents the dispersion and polarization contributions to the T-model potential. ΔE^r could be determined from both theoretical and experimental data. Our previous experience has shown that a calibration of the incomplete potential to the properties related to intermolecular interactions, such as the second virial coefficients ($B(T)$), dimerization energies or ϵ potential energy of liquid etc., seems to be the most appropriate choice. ΔE^r takes the following form:

$$\Delta E^r = -\sum_{i\epsilon A}\sum_{j\epsilon B} C^6_{ij} F_{ij}(R_{ij}) R^{-6}_{ij} \tag{3}$$

where

$$F_{ij}(R_{ij}) = \exp\left\{-\left(1.28R^0_{ij}/R_{ij}-1\right)^2\right\}, \text{ if}$$
$$R_{ij} < 1.28R^0_{ij} = 1, \text{ elsewhere} \tag{4}$$

and

$$C^6_{ij} = C_6\frac{3}{2}\frac{\alpha_i\alpha_j}{(\alpha_i/N_i)^{1/2}+(\alpha_j/N_j)^{1/2}} \tag{5}$$

R^0_{ij} in Eq. (4) is the sum of van der Waals radii of interacting atoms. Eq. (5) is the Slater–Kirkwood relation. α_i and N_i in Eq. (5) denote the atomic polarizability and the number of valence electrons of the corresponding atom, respectively. F_{ij} (R_{ij}) in Eq. (4) is a damping function, introduced to correct the behavior of R^{-6}_{ij} at short R_{ij} distance. Only C_6 in Eq. (5) is unknown.

In our experience, the values of C_6 could be varied within a wide range and careful variation of C_6 seems not lead to significant changes in the potential energy surface (PES). For some microsolvated systems, the values of C_6 were determined by adjusting the C_6 parameters to reproduce the interaction energies computed from ab initio calculations. This includes, for example, the phenol–H_2O 1:1 complex [27], benzoic acid dimer ($(BA)_2$), the BA–H_2O 1:1 complex [29] and $(NH_2OH)_2$ [28]. The calibration procedure employed in the present work consists of three basic steps as follows: (a) the T-model parameters for the Gdm^+ and FmO^- ions, with C_6=1.0, were applied in the calculations of the equilibrium structures and interaction energies of the Gdm^+–H_2O, FmO^-–H_2O and Gdm^+–FmO^- 1:1 complexes in the gas phase; (b) all the global minimum energy geometries predicted by the T-model potentials were reoptimized using ab initio calculations at the MP2/6-311++G(d,p) level for the Gdm^+–H_2O and Gdm^+–FmO^- complexes, and at the MP2/6-311++G(2d,2p) level for the FmO^-–H_2O complex. The interaction energies of the reoptimized geometries were corrected using conventional single point counterpoise correction of the basis set superposition error (BSSE) [34]; (c) the C_6 parameters for the complexes were readjusted, using the corresponding MP2 interaction energies as guide lines. The computed C_6 parameters for the Gdm^+–H_2O, FmO^-–H_2O and Gdm^+–FmO^- complexes are 1.13, 1.54 and 2.48, respectively. The T-model parameters for Gdm^+, FmO^- and water can be sent on request.

2.2. MD simulations

In order to provide insights into the structures and energetic of the H-bond networks of water in the first hydration shell of the Gdm^+ and FmO^- ions, as well as the Gdm^+–FmO^- complex, the T-model potentials computed in the previous section were applied in NVE-MD simulations of $[Gdm^+]_{aq}$, $[FmO^-]_{aq}$ and $[Gdm^+–FmO^-]_{aq}$ at 298 K. In MD simulations in general, an ion or an ion-pair was put at the center a cubic box subject to periodic boundary conditions. The solute was surrounded by five hundred water molecules, with the density of the aqueous solutions maintained at 1.0 g/cm^3. The cutoff radius was half of the box length. The Ewald summation was applied to account for the long-range Coulomb interaction. Fifty thousand MD steps of 0.0005 ps were devoted to equilibration and one hundred thousand steps to property calculations. The primary energetic results obtained from MD simulations were the average solute–solvent interaction energies ($\langle E_{aq}^{solu-solv}\rangle$) and the average solvent–solvent interaction energies ($\langle E_{aq}^{solv-solv}\rangle$), as well as the average potential energy of aqueous solutions ($\langle E_{aq}^{pot}\rangle$). These energy values were the results of the average over the MD steps and the number of solvent molecules. They are summarized in Table 1, together with all the MD simulations conditions employed in the present study.

To fulfill all the major objectives, six series of MD simulations were performed in the present study. MD-$[Gdm^+]_{aq}$ and MD-$[FmO^-]_{aq}$ represent MD simulations, in which single ions and water molecules were considered. In MD simulations of $[Gdm^+–FmO^-]_{aq}$, the most stable configuration of the Gdm^+–FmO^- 1:1 complex in the gas phase, structure (a) in Fig. 3, was chosen as a representative ion-pair.

It should be mentioned that, for the dimerization of alanine dipeptide in aqueous solutions [35], a relatively large free energy barrier corresponding to the intermediate state is characterized by a single hydration layer of interstitial water molecules which separates the close-contact dimer from the solvent-separated structure. It is, therefore, of interest to study the hydration structures and stability of such an intermediate state in $[Gdm^+–FmO^-]_{aq}$. Since our preliminary PMF calculations on $[Gdm^+–FmO^-]_{aq}$ [36] revealed two shallow minima at $R_{C\cdots C}\approx$ 3.9 and 6.3 Å on the free energy profile, we adopted these two configurations in the present MD simulations. They correspond to the close-contact and solvent-separated Gdm^+–FmO^- structures, respectively; the two minima are separated by a very low free energy barrier. In the present study, MD-$[Gdm^+–FmO^-]^{R=X}_{aq,\ frozen}$ symbolizes the MD simulations, in which structure (a) with $R_{C\cdots C}$=X was frozen in the course of MD simulations. Therefore, MD-$[Gdm^+–FmO^-]^{R=X}_{aq,\ frozen}$ with $R_{C\cdots C}$=3.9 and 6.3 Å could assimilate, respectively, the initial and intermediate states, in which the H-bonds in the close-contact ion-pair are disrupted by water molecules in the interstitial H-bond network.

The stability of the close-contact and solvent-separated Gdm^+–FmO^- complexes in aqueous solutions was discussed based on the results of MD-$[Gdm^+–FmO^-]^{R=X}_{aq,\ free}$. In MD-$[Gdm^+–FmO^-]^{R=X}_{aq,\ free}$, two consecutive equilibration steps were carried out before property calculations took place. In the first equilibration step, the Gdm^+–FmO^- complex with $R_{C\cdots C}=X$ was treated as a supermolecule, in which both Gdm^+ and FmO^- ions were not allowed to move in the course of MD simulations. After water molecules were well-equilibrated, all molecules inside the simulation box, including the Gdm^+ and FmO^- ions, were allowed to freely move in the second equilibration.

The hydration structures in $[Gdm^+]_{aq}$, $[FmO^-]_{aq}$ and $[Gdm^+–FmO^-]_{aq}$ were primarily analyzed using the atom–atom pair correlation functions ($g(R)$) and the average running coordination number ($n(R)$). The three-dimensional structures of the H-bond networks of water in the aqueous solutions were visualized using the PDO and PDH maps. In the present case, they represent static pictures of the H-bond networks of water in the first hydration shells of solutes. In the constructions of the PDO and PDH maps, the molecular plane of solute was assumed to coincide with the XY plane of the simulation box (with Z=0 Å). The volumes above

Table 1
MD simulations parameters and the results for $[Gdm^+]_{aq}$, $[FmO^-]_{aq}$ and $[Gdm^+–FmO^-]_{aq}$

MD	L	$\langle E_{aq}^{pot}\rangle$	$\langle E_{aq}^{solu-solv}\rangle$	$\langle E_{aq}^{solv-solv}\rangle$	$\langle E_{aq}^{solu-solu}\rangle$
$[Gdm^+]_{aq}$	24.6865	−30.99±0.16	−0.9	−29.6	–
$[FmO^-]_{aq}$	24.6729	−31.35±0.16	−1.1	−29.6	–
$[Gdm^+–FmO^-]^{R=3.9}_{aq,\ frozen}$	24.7273	−31.90±0.17	−0.9	−29.4	−480.8*
$[Gdm^+–FmO^-]^{R=3.9}_{aq,\ free}$	24.7273	−31.94±0.16	−1.0	−29.5	−457.0
$[Gdm^+–FmO^-]^{R=6.3}_{aq,\ frozen}$	24.7273	−31.98±0.17	−1.5	−29.2	−256.5*
$[Gdm^+–FmO–]^{R=6.3}_{aq,\ free}$	24.7273	−31.96±0.17	−0.6	−29.1	−120.4

L—simulation box lengths.
$\langle E_{aq}^{pot}\rangle$—average potential energy of aqueous solution.
$\langle E_{aq}^{solu-solv}\rangle$—average solute–solvent interaction energy.
$\langle E_{aq}^{solv-solv}\rangle$—average solvent–solvent interaction energy.
$\langle E_{aq}^{solu-solu}\rangle$—average solute–solute interaction energy.
*—$\Delta E_{T\text{-}model}$ for the Gdm^+–FmO^- 1:1 complex in the gas phase.
Energies are in kJ/mol and distances are in Å.

and below the molecular plane of solute were divided into layers, with the thickness of 1 Å. In each layer, the PDO and PDH maps were computed at 61×61 grid intersections, by following the trajectories of oxygen and hydrogen atoms of water in the course of MD simulations. The PDO and PDH maps were represented by contour lines [37]. For simplicity, the maximum and minimum values of the contour lines, as well as the contour interval were chosen to be the same for all the PDO and PDH maps.

In order to obtain insights into the interaction energy distributions in $[Gdm^+]_{aq}$, $[FmO^-]_{aq}$ and $[Gdm^+–FmO^-]_{aq}$, a similar approach was adopted to construct the AWPD, WWPD and AW-WWPD maps. The AWPD maps were derived from the average interaction energies between the water molecules at the grid intersections and the ion or ion-pair, whereas the WWPD maps were computed based on the average interaction energies between the water molecules at the grid intersections and all other water molecules in aqueous solutions. In the present study, the AW-WWPD maps represent the average potential energy landscapes of the H-bond networks of water. They were computed by combination of the AWPD and WWPD maps [16]. Only the negative interaction energies were displayed in the AWPD, WWPD and AW-WWPD maps.

Since the dynamic behavior of water molecules in the H-bond networks was one of our main objectives, additional MD analyses were made. Due to the fact that the mobility of water molecules depends on the transition energy barriers, which could be estimated from the average potential energy landscapes, the AWPD, WWPD and AW-WWPD maps were examined in details. Various cross section plots of the average potential energy landscapes were generated by taking vertical slices along predefined profile lines, through the surfaces of the AW-WWPD maps, as well as the AWPD and WWPD maps [16]. In the present study, the cross section plots computed from the longitudinal profile lines could be associated with the transition energy barriers to water exchange within, as well as between, the H-bond networks ($\langle E_{aq}^{L} \rangle$). Whereas those derived from the transverse profile lines are related to the transition energy barriers to water exchange between the H-bond networks and the outsides ($\langle E_{aq}^{T} \rangle$).

It should be augmented that, when a particular water molecule leaves the first hydration shell, its place is occupied nearly simultaneously by another water molecule. Therefore, the residence time has been frequently used in the discussion of the dynamic behavior of water molecules in the first hydration shells of solutes [38]. The measured residence times seem to be very sensitive to the methods used, and could be approximated in general by MD simulations and NMR experiments [39]. However, both approaches have advantages and disadvantages [38,40]. For examples, due to the fact that the H-bond formations and disruptions take place very often and very fast in the first hydration shell of solutes, the residence times derived from MD simulations could vary in a wide range [40], depending on the path taken by individual water molecule; whereas NMR experiments can more effectively detect the long-lived hydration water [38]. From our literature survey, there have been various approaches to calculate the residence times from MD simulations [39–41]. The one proposed by Impey et al. [41] seems to be relatively straight forward and widely used, especially for spherical symmetric solutes such as monovalent ions [41,42]. Since the ions and ion-pair considered here are more complicated and our intention is only to characterize the mobility of water molecules in the H-bond networks in terms of the average potential energy landscapes, we decided to adopt our previous definition [16] in the present study. The so-called "the longest H-bond lifetime" ($\tau_{A-H\cdots B,\ max}$) was approximated from the percentage of the MD steps, during which a specific pair of H-bond donor and acceptor coming close enough to continuously engage in H-bond. The H-bond donor and acceptor were considered to engage in H-bond when the donor–acceptor distance was shorter than 4 Å [2,43]. Our attention was focused on cyclic-bifurcated H-bonding features, since preliminary MD simulations showed that they dominate in $[Gdm^+]_{aq}$, $[FmO^-]_{aq}$ and $[Gdm^+–FmO^-]_{aq}$.

3. Results and discussion

3.1. Equilibrium structures in the gas phase

Since the main objectives of the present work were to investigate hydration structures and stability of the ions and the ion-pair in aqueous solutions, the analysis of the equilibrium structures and interaction energies in the gas phase was made only to sample check the potential energy surfaces, as well as to test the applicability and reliability of the computed T-model potentials. This is to ensure that the T-model potentials will give reasonable results when applied in MD simulations. Due to the fact that different theoretical approaches yield different results, comparisons with available theoretical and experimental data were not made rigorously in the following subsections.

The absolute and some low-lying minimum energy geometries for the $Gdm^+–H_2O$, $FmO^-–H_2O$ and $Gdm^+–FmO^-$ complexes, computed from the T-model potentials, are illustrated in Figs. 1–3, respectively. $\Delta E_{T\text{-model}}$ and some characteristic H-bond distances and angles, together with the corresponding results from MP2 calculations, are included in the figures for comparison.

3.1.1. The $Gdm^+–H_2O$ complex

In general, the results on the $Gdm^+–H_2O$ 1:1 complex are as expected namely, a cyclic-bifurcated N–H···Ow H-bond structure, structure (a) in Fig. 1, represents the global minimum energy geometry in the gas phase. Both N–H···Ow H-bonds in structure (a) are identical, with two N–H groups of Gdm^+ acting as proton donors toward the oxygen atom of water. The Gdm^+ and H_2O molecular planes are

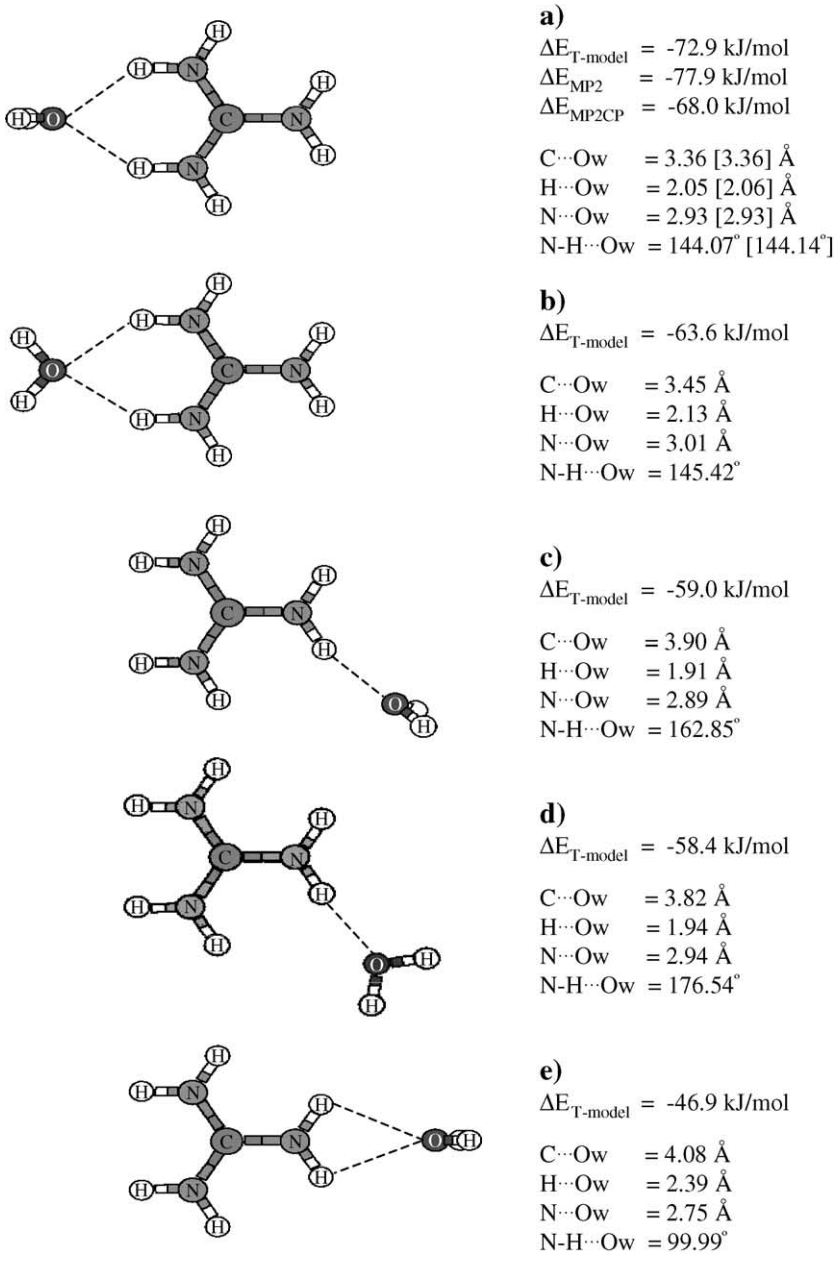

Fig. 1. Equilibrium structures and interaction energies of the Gdm^+–H_2O 1:1 complex in the gas phase computed from the T-model potentials. [···] the values obtained from MP2/6-311++G(d,p). The numbering system of Gdm^+ is as follows:

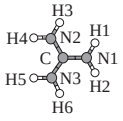

perpendicular, with the N–H···Ow H-bond distance and $\Delta E_{\text{T-model}}$ of 2.93 Å and −72.9 kJ/mol, respectively. Starting from structure (a), MP2/6-311++G(d,p) yielded the same structure. The BSSE corrected interaction energy of structure (a), ΔE_{MP2CP} in Fig. 1, is −68.0 kJ/mol. The T-model predicted structure (b) to be 9.3 kJ/mol less stable than structure (a). For structure (b), the Gdm^+ and H_2O molecular planes are coplanar, with the cyclic-bifurcated N–H···Ow H-bond distance and $\Delta E_{\text{T-model}}$ of 3.01Å and −63.6 kJ/mol, respectively. The relative orientations of water molecules in structures (a) and (c), as well as in structures (b) and (d), are similar. However, the water molecules in structures (c) and (d) are H-bonded to the Gdm^+ ion through a single N–H···Ow H-bond, with the Gdm^+ and H_2O molecular planes perpendicular and coplanar with each other, respectively. $\Delta E_{\text{T-model}}$ of structures (c) and (d) are almost the same, −59.0 and −58.4 kJ/mol, respectively. The N–H···Ow H-bond distance in

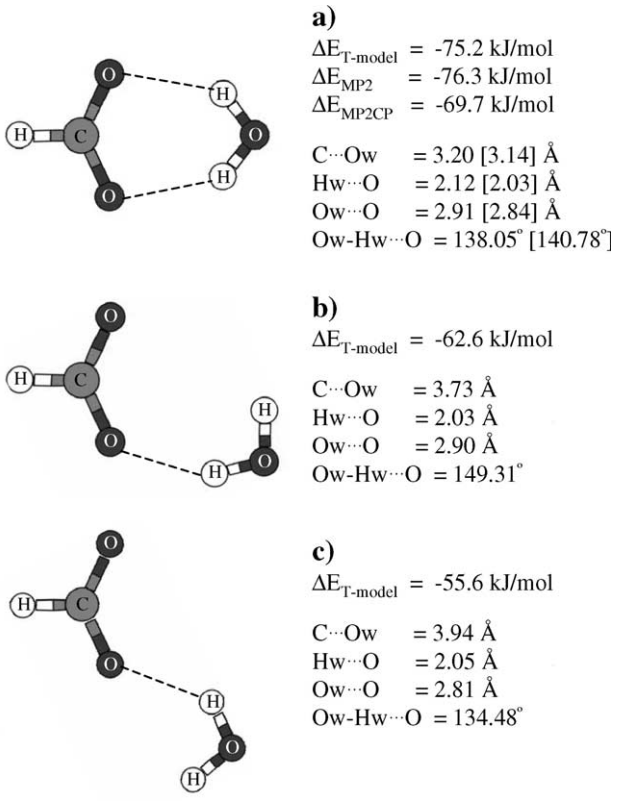

Fig. 2. Equilibrium structures and interaction energies of the FmO^-–H_2O 1:1 complex in the gas phase computed from the T-model potentials. [···] the values obtained from MP2/6-311++G(2d,2p). The numbering system of FmO^- is as follows:

structure (d) is slightly longer than structure (c). Structure (e) represents another type of cyclic-bifurcated H-bond in the Gdm^+–H_2O 1:1 complex, with $\Delta E_{T\text{-model}}$ and the N–H···Ow H-bond distance of −46.9 kJ/mol and 2.75 Å, respectively.

Only limited number of low-lying minimum energy geometries of the Gdm^+–H_2O 1:1 complex were reported in the literature [44–46]. Based on the OPLS potentials and ab initio calculations with the 6-31G(d) basis set [46], structure (a) possesses the interaction energies of −74.4 and −76.1 kJ/mol, respectively. Whereas the AM1/TIP3P [45] and ab initio calculations [46] predicted the C···Ow distances to be 3.22 and 3.41 Å, respectively. Structure (d) was inferred from the OPLS potentials and ab initio calculations to be an additional minimum energy geometry, with the interaction energies of −66.0 and −57.7 kJ/mol, respectively [46].

3.1.2. The FmO^-–H_2O complex

The T-model potential predicted a cyclic-bifurcated Ow–Hw···O H-bond structure, structure (a) in Fig. 2, to be the absolute minimum energy geometry for the FmO^-–H_2O 1:1 complex. Structure (a) consists of two symmetric Ow–Hw···O H-bonds, with water molecule acting as proton donors toward the COO^- group. Both Ow–Hw···O H-bond distances are 2.91 Å, with $\Delta E_{T\text{-model}}$ of −75.2 kJ/mol. MP2/6-311++G(2d,2p) geometry optimization predicted the same structure, with slightly shorter Ow–Hw···O H-bond distance. ΔE_{MP2CP} for structure (a) is −69.7 kJ/mol. The second and third low-lying minimum energy geometries for the FmO^-–H_2O 1:1 complex are represented by a single Ow–Hw···O H-bond formation, with $\Delta E_{T\text{-model}}$ of −62.6 and −55.6 kJ/mol, respectively; the Ow–Hw···O H-bond distances are 2.90 and 2.81 Å, respectively.

Three low-lying minimum energy geometries similar to ours were reported for the FmO^-–H_2O [47–50] and AcO^-–H_2O 1:1 complexes [45]. The interaction energy of structure (a) was estimated by ab initio calculations at the HF/6-31G(d,p) level, plus the counterpoise and dispersion corrections, to be −83.6 kJ/mol [48], whereas the structures similar to structures (b) and (c) were about −71.1 kJ/mol [48]. The C···Ow distances for these structures are in good agreement with the T-model results, 3.23, 3.91 and 3.92 Å, respectively [47]. Ab initio calculations at the HF/6-31+G(d) level [49] yielded the interaction energies of −76.1,−64.0 and −61.0 kJ/mol, respectively.

3.1.3. The Gdm^+–FmO^- complex

Two equilibrium geometries for the Gdm^+–FmO^- 1:1 complex were generated from the T-model potential. The absolute minimum energy geometry is represented by a coplanar cyclic arrangement of the N–H···O H-bonds, structure (a) in Fig. 3. The two N–H···O H-bonds are identical, with the N–H groups of the Gdm^+ ion acting as proton donors toward the COO^- group of FmO^-. $\Delta E_{T\text{-model}}$ of structure (a) is −480.8 kJ/mol, with the N–H···O H-bond distances of 2.74 Å. Starting from structure (a), MP2/6-311++G(d,p) geometry optimization yielded the same structure, with the BSSE corrected interaction energy of −480.1 kJ/mol; the N–H···O H-bond distances are slightly smaller than the T-model result. Structure (a) is similar to a bidentate H-bonding structure reported in Ref. [51], in which ab initio calculations at MP2/6-31+G(d,p)//MP2/6-31+G(d,p) level predicted the interaction energy to be −542.6 kJ/mol and the N–H···O H-bond distances of 2.6 Å. Another type of cyclic-bifurcated N–H···O H-bonds was predicted by the T-model potential, structure (b) in Fig. 3. Structure (b) possesses the interaction energy and the N–H···O H-bond distances of −431.4 kJ/mol and 2.62 Å, respectively.

In order to provide insight into the accuracy of the MP2 results reported in this section, geometry optimizations on the ions and the 1:1 complexes were performed at the HF level with the same basis sets. It was found that, at the HF level, the covalent bond lengths were systematically shorter, 0.03 Å at most; whereas the bond angles did not change significantly. For all the 1:1 complexes, the H-bond distances obtained from ab initio calculations at the HF level were systematically longer, 0.16 Å at most. The latter represents general trend when the effects of electron correlation were neglected;

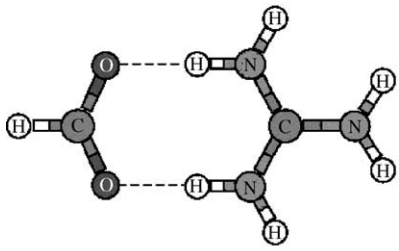

a)

$\Delta E_{T\text{-model}}$ = -480.8 kJ/mol
ΔE_{MP2} = -497.2 kJ/mol
ΔE_{MP2CP} = -480.1 kJ/mol

C···C = 3.93 [3.83] Å
H···O = 1.73 [1.63] Å
N···O = 2.74 [2.63]Å
N-H···O = 177.67° [177.69°]

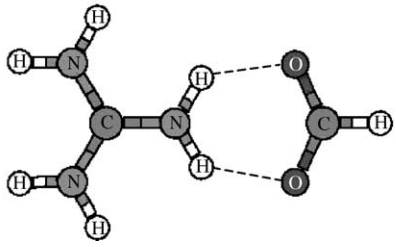

b)

$\Delta E_{T\text{-model}}$ = -431.4 kJ/mol

C···C = 4.22 Å
N···C = 2.88 Å
H···O = 1.86 Å
N···O = 2.62 Å
N-H···O = 129.52°

Fig. 3. Equilibrium structures and interaction energies of the Gdm^+–FmO^- 1:1 complex in the gas phase computed from the T-model potentials. [···] the values obtained from MP2/6-311++G(d,p). The numbering system of Gdm^+–FmO^- is as follows:

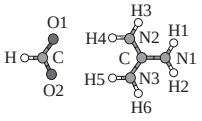

additional attractive interaction is obtained when ab initio calculations take into account the dispersion interaction properly. This also implies that the basis sets employed in the present MP2 calculations are quite reasonable, leading to correct effects of electron correlation. It should also be stressed that the T-model employed in the present work takes into account the effects of electron correlation in an approximate way, using the Slater–Kirkwood relation and the C_6 parameter. This considerably reduces computational efforts, especially for large H-bond and aromatic systems, in which the effects of electron correlation cannot be neglected [27,29,30]. The T-model has been proved to be an appropriate choice for the situations, in which the numerical accuracy and the computational facility are to be balanced.

3.2. MD simulations

$\langle E_{aq}^{pot}\rangle$, $\langle E_{aq}^{solu-solv}\rangle$, $\langle E_{aq}^{solv-solv}\rangle$ and $\langle E_{aq}^{solu-solu}\rangle$ are included in Table 1, together with the conditions employed in MD simulations. In order to limit the number of figures, only some selected PDO, AWPD and AW-WWPD maps, as well as the corresponding cross section plots, are illustrated. Characteristic high-density contour areas on the PDO, AWPD and AW-WWPD maps are labeled with letters. To compare the transition energy barriers to water exchanges ($\langle E_{aq}^{L}\rangle$ and $\langle E_{aq}^{T}\rangle$) at various H-bond networks, the lowest energy minima on the AW-WWPD cross section plots were set to 0 kJ/mol [16].

Since the ions and the ion-pair considered in the present work possess symmetries, some H-bond networks are equivalent. To simplify the discussion, equivalent H-bond networks were categorized and analyzed. $\tau_{A\text{-}H\cdots B,\ max}$ obtained from MD-$[Gdm^+]_{aq}$, MD-$[FmO^-]_{aq}$ and MD-$[Gdm^+\text{–}FmO^-]_{aq,\ frozen}^{R=X}$ are summarized in Table 2, together with some characteristic $\langle E_{aq}^{T}\rangle$.

3.2.1. $[Gdm^+]_{aq}$

Fig. 4 shows $g(R)$ and $n(R)$ directly related to the H-bonds in $[Gdm^+]_{aq}$, together with the PDO, AWPD and AW-WWPD maps and the cross section plots. The H-bond networks at **A**, **B** and **C** are equivalent due to the symmetry of the Gdm^+ ion. Therefore, only two types of H-bond networks are to be discussed in $[Gdm^+]_{aq}$. The representative examples are the H-bond networks in the areas between H4 and H5 and between H1 and H2 in Fig. 1. They are regarded as the H-bond network types **I** and **II**, respectively.

The main peak of $g(R_{C\cdots Ow})$ in Fig. 4a is split into two peaks, corresponding to the H-bond network types **I** and **II**, respectively. The peak height of $g(R_{C\cdots Ow})$ at R_{max}=3.43 Å is slightly lower than that at R_{max}=4.09 Å. The first peak could be attributed to the H-bonding features in structures (a) and (b), whereas the second one accounts for structures (c), (d) and (e) in Fig. 1. The N–H···Ow H-bonds in $[Gdm^+]_{aq}$ seem to be quite strong, as seen from the structures of the main peaks of $g(R_{N\cdots Ow})$ and $g(R_{H\cdots Ow})$ in Fig. 4a. $g(R_{N\cdots Ow})$ indicates that, at R_{max}=2.90 Å, there is about one (1.2) water molecule in close-contact or H-bonded to each N–H group of Gdm^+, and about eight (7.8) water molecules in the first hydration shell at 4.09 Å.

The preferential hydration sites and the three-dimensional structures of the H-bond networks of water in

Table 2
$\tau_{\text{type X, max}}$ and some $\langle E_{aq}^{T} \rangle$ obtained from MD simulations of $[Gdm^{+}]_{aq}$, $[FmO^{-}]_{aq}$ and $[Gdm^{+}-FmO^{-}]_{aq}$

X	MD–$[Gdm^{+}]_{aq}$		MD–$[FmO^{-}]_{aq}$		MD–$[Gdm^{+}-FmO^{-}]^{R=3.9}_{aq,\ frozen}$		MD–$[Gdm^{+}-FmO^{-}]^{R=6.3}_{aq,\ frozen}$	
	$<\Delta E_{aq}^{T}>$	τtype X, max	$<\Delta E_{aq}^{T}>$	τtype X, max	$<\Delta E_{aq}^{T}>$	τtype X, max	$<\Delta E_{aq}^{T}>$	τtype X, max
I	101.8	8.52	–	–	86.3	6.92	101.5	10.04
II	76.8	11.11	–	–	34.8	6.98	84.3	14.29
III	–	–	86.7	1.84	–	-	-	-
IV	–	–	26.5	1.17	–	-	-	-
V	–	–	–	–	24.3	1.41	23.7	8.96
VI	–	–	–	–	–	-	102.2–103.8	18.14

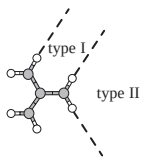

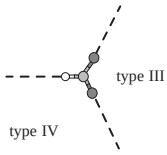

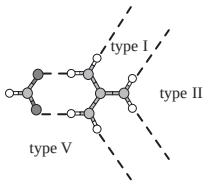

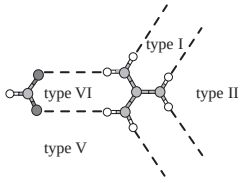

Energies are in kJ/mol and time is in ps.

$[Gdm^{+}]_{aq}$ are visualized and analyzed using the PDO, AWPD and AW-WWPD maps in Fig. 4b to d. They are quite well-defined which support the results of $g(R)$ in general. The three most important H-bond networks seem to be all connected and located on the Gdm^{+} molecular plane. The H-bonding features at these H-bond networks seem to include all structures in Fig. 1. According to the contour densities on the PDO maps in Fig. 4b and c, the H-bond network type **I** appeared with higher probability compared to the H-bond network type **II**. In other words, the H-bonding features in structures (a) and (b) were observed with higher frequencies in MD simulations, compared to structures (c), (d) and (e). Fig. 4d suggests the boundary of the first hydration shell of Gdm^{+} to be in the layer with $Z=2$ to 3 Å.

The structures of the average potential energy landscapes in Fig. 4e to h show that the H-bond network types **I** and **II** are different in detail. The longitudinal AW-WWPD cross section plot of the H-bond network type **I** in Fig. 4e reveals slightly smaller transition energy barriers ($\langle E_{aq}^{L} \rangle$) at the basin, compared to those of the H-bond network type **II** in Fig. 4g. This suggests that water molecules could move or exchange easier within the H-bond network type **I**. It was also recognized in Fig. 4e and f that, in the vicinity of the highest contour density of the H-bond network type **I**, the AWPD cross section plots are lower than the WWPD cross section plots and the structures of the AW-WWPD cross section plots are determined by the shape of the AWPD cross section plots. This is opposite to the situations in the H-bond network type **II**. These pieces of information will be used to characterize the energy contributions to the stability of the close-contact Gdm^{+}–FmO^{-} complex in aqueous solutions. The transverse AW-WWPD cross section plots in Fig. 4f and h reveal that the motions of water molecules inside the H-bond network types **I** and **II** are confined in narrow interaction energy valleys of about 3 Å, with $\langle E_{aq}^{T} \rangle$ for the water exchange between the H-bond networks and the outsides of about 102 and 77 kJ/mol, respectively.

As mentioned earlier that the dynamic behavior of specific water molecules at the H-bond networks could be inferred from the average potential energy landscapes [16] and vice versa. Therefore, the detail information on the structures of the average potential energy landscapes could be useful to identify the paths taken by individual water molecules. It should also be emphasized that, based on our criteria, the minima on the average potential energy landscapes, such as AW-WWPD maps, are associated with the low-lying interaction energy states, which were occupied by water molecules in the course of MD simulations. Furthermore, since the probability and the duration for a water molecule to occupy an interaction energy state depend upon the hydration dynamics of individual water molecule, as well as the transition energy barriers interconnecting the interaction energy states, it is reasonable to assume that the structures of the average potential energy landscapes define the H-bond lifetime. Since, by definition, $\tau_{\text{A-H\_B, max}}$ represents the longest H-bond lifetime, in which a specific water molecule is trapped inside the H-bond network of interest, one could identify the water molecule which takes the rate-determining water exchange path; by assuming that the water molecule with the highest $\tau_{\text{A-H\_B, max}}$ enters the H-bond network by taking the path with the highest transition energy barriers. With this approach it is also possible to predict the rate-determining water exchange path at the H-bond networks. The assumption could be applied in the study of the reaction path, on which a reactive substrate is trapped long enough at functional group of receptor, in order that a specific chemical reaction could take place.

According to the above discussions on the AW-WWPD cross section plots, especially $\langle E_{aq}^{T} \rangle$, one could anticipate that $\tau_{\text{type I, max}}$ is larger than $\tau_{\text{type II, max}}$. In the present case, however, such a direct comparison is not appropriate. Since, based on our criteria for the bifurcated H-bond formation, the area occupied by the H-bond network type **II** is more than twice larger than that of the H-bond network type **I**. We will, therefore, focus our attention on the effects of the ion-pair

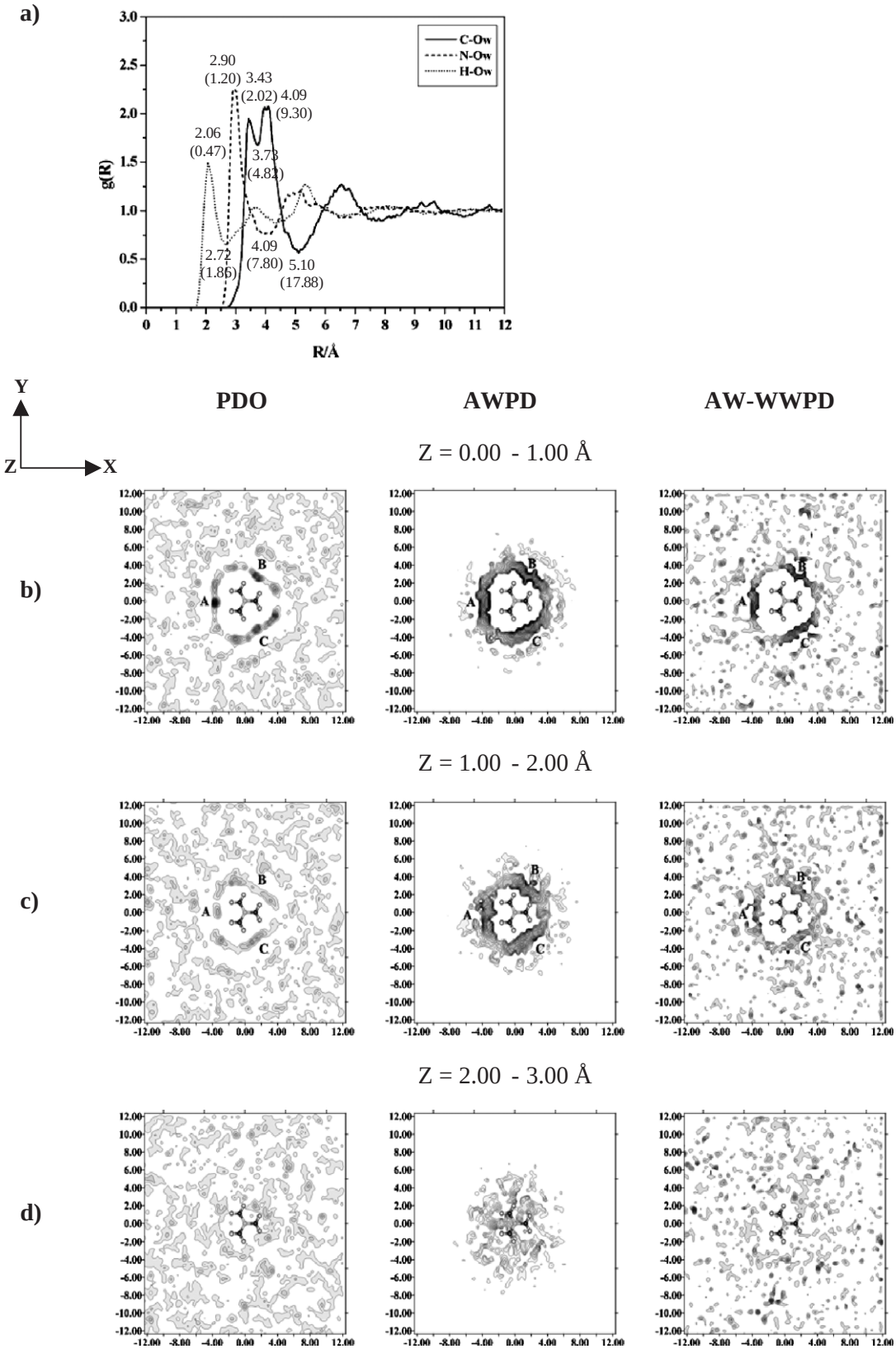

Fig. 4. Selected structure and energetic results obtained from MD-$[Gdm^{+}]_{aq}$. (a) $g(R)$; characteristic distances are given, with $n(R)$ in parentheses. (b–d) The PDO, AWPD and AW-WWPD maps. (e–h) Cross section plots computed from longitudinal and transverse profile lines. —: The AW-WWPD cross section plot. ----: The AWPD cross section plot. ·····: The WWPD cross section plot. *X*-, *Y*- and *Z*-axes are in Å; energies are in kJ/mol.

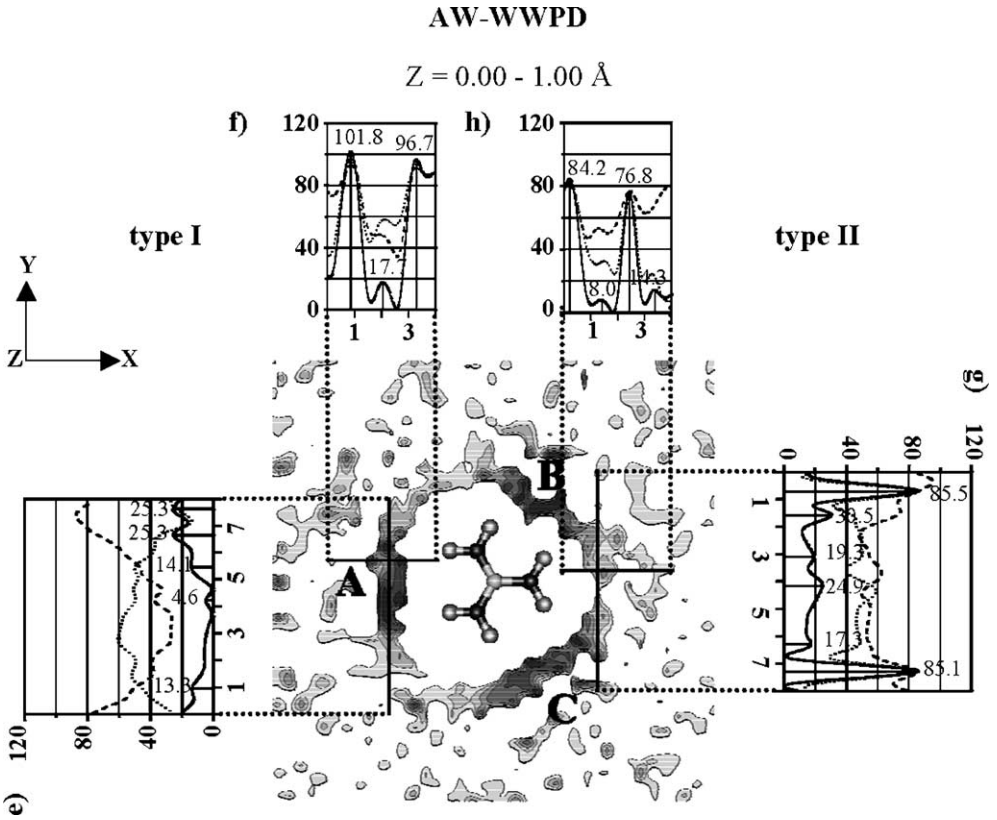

Fig. 4 (*continued*).

formation on the longest H-bond lifetimes at equivalent H-bond networks. In Table 2, $\tau_{\text{type I, max}}$ and $\tau_{\text{type II, max}}$ are about 9 and 11 ps, respectively, comparable with the approximated residence time at Na^+ in $[NaCl]_{aq}$ of 15 ps [42].

In order to obtain information on the accuracy of $\tau_{\text{A-H..B, max}}$, additional comparisons have to be made. In the present case, we performed MD analyses on pure water and observed some interesting results. It was found that, based on our approach, the longest H-bond lifetime at the H atom of water was 8.7 ps, whereas the one at the O atom was 3.2 ps. These are compared well with the H-bond residence times reported based on NMR experiment of about 8 ps [52] and MD simulations of 4.5 ps [41]. The H-bond mean residence times of water within the first hydration shell of a water molecule were reported to be ranging from 2.5 to 10.0 ps in Ref. [53]. It should be added that, from the literature survey [41,52–54], the values of the H-bond lifetime or the H-bond residence time are sensitive to the definitions, as well as the methods employed in the investigations. It is, therefore, more appropriate to discuss and compare the results using pure water as a reference. In the present work, it is obvious that the reported values of $\tau_{\text{A-H..B, max}}$ are reasonable relative to the pure water, and our definition has been proved to be applicable.

3.2.2. $[FmO^-]_{aq}$

Selected results on MD-$[FmO^-]_{aq}$ are illustrated in Fig. 5. g($R_{C\cdots Ow}$)in Fig. 5a shows the main peak at R_{max}=3.55 Å, with n(R_{max})=4.15. The latter suggests about four water molecules in close-contact with FmO^-. The position of the main peak of $g(R_{C\cdots Ow})$ is slightly too long to assign to structure (a) and slightly too short to be structure (b) in Fig. 2. This makes believe that the average H-bonding feature in $[FmO^-]_{aq}$ lies between structures (a) and (b). $g(R_{O\cdots Ow})$ in Fig. 5a reveals about two (1.82) water molecules H-bonding directly to each oxygen atom of FmO^-, with the Ow–Hw···O H-bond distance of 2.96 Å. The H-bond networks of water at the C–H group of FmO^- are less well-defined compared to the COO^- group, as seen from the size and shape of the main peak of $g(R_{H\cdots Ow})$ in Fig. 5a.

For $[FmO^-]_{aq}$, three well-defined H-bond networks are seen on the PDO maps. They are labeled with **D**, **E** and **F** in Fig. 5b and c. The H-bond network at **E** is located slightly above the FmO^- molecular plane, and is regarded as the H-bond network type **III** in the present study. The H-bond networks at **D** and **F** are equivalent. Both of them are seen on the FmO^- molecular plane, and are categorized as the H-bond network type **IV**. The H-bond network at **E** spans from the O1 to O2 atoms, with the contour density slightly higher than that at **D** and **F**. Fig. 5d shows the boundary of the first hydration shell of FmO^-, in the layer with Z=2 to 3 Å.

The longitudinal AW-WWPD cross section plots in Fig. 5e and g reveal that the H-bond networks at **D**, **E** and **F** are quite well-connected. Their structures suggest that, on average, water molecule in the H-bond network type **III** could move or exchange within a wider range, compared to

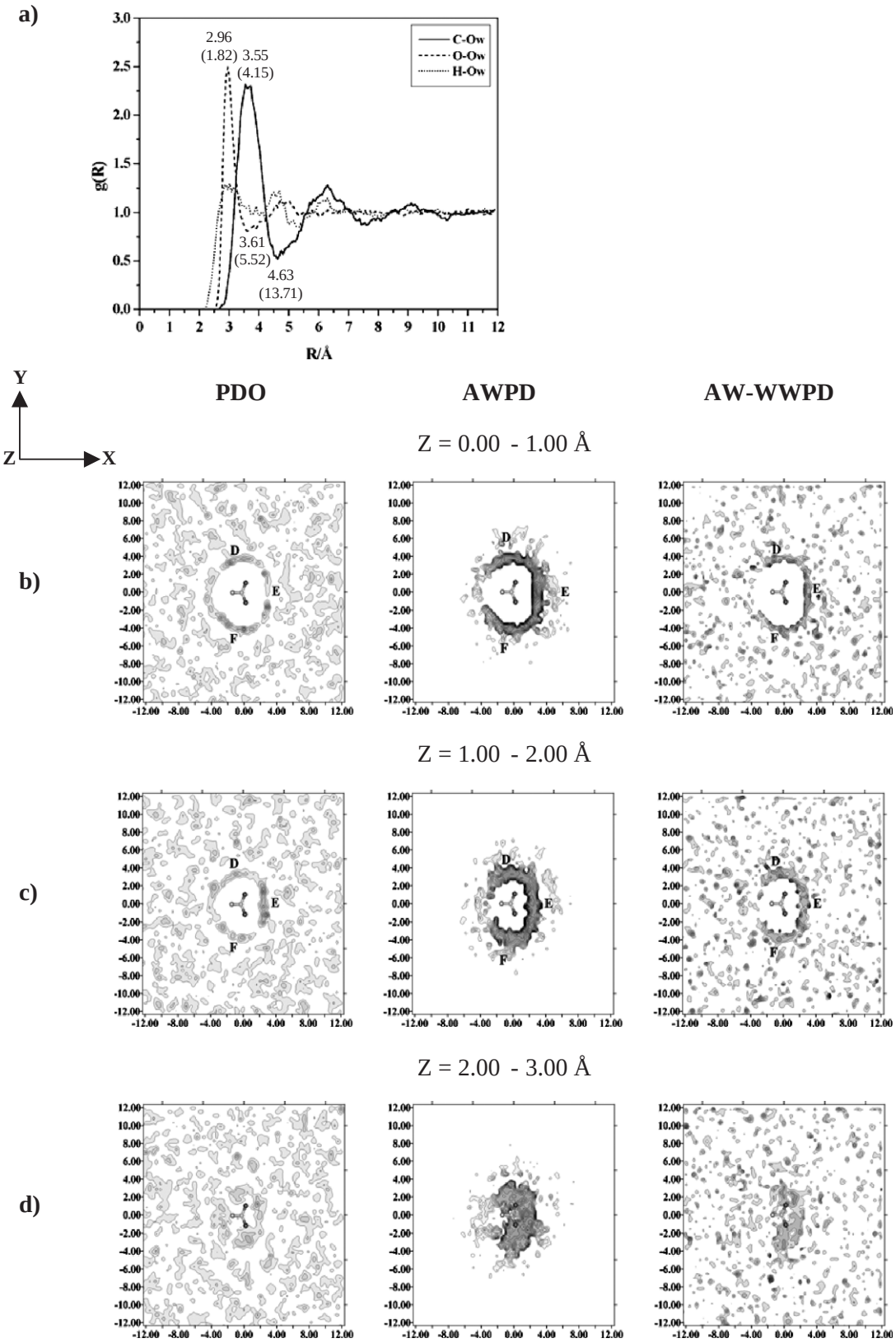

Fig. 5. Selected structure and energetic results obtained from MD-$[FmO^-]_{aq}$. (a) $g(R)$; characteristic distances are given, with $n(R)$ in parentheses. (b–d) The PDO, AWPD and AW-WWPD maps. (e–h) Cross section plots computed from longitudinal and transverse profile lines. —: The AW-WWPD cross section plot. ----: The AWPD cross section plot. ·····: The WWPD cross section plot. *X*-, *Y*- and *Z*-axis are in Å; energies are in kJ/mol.

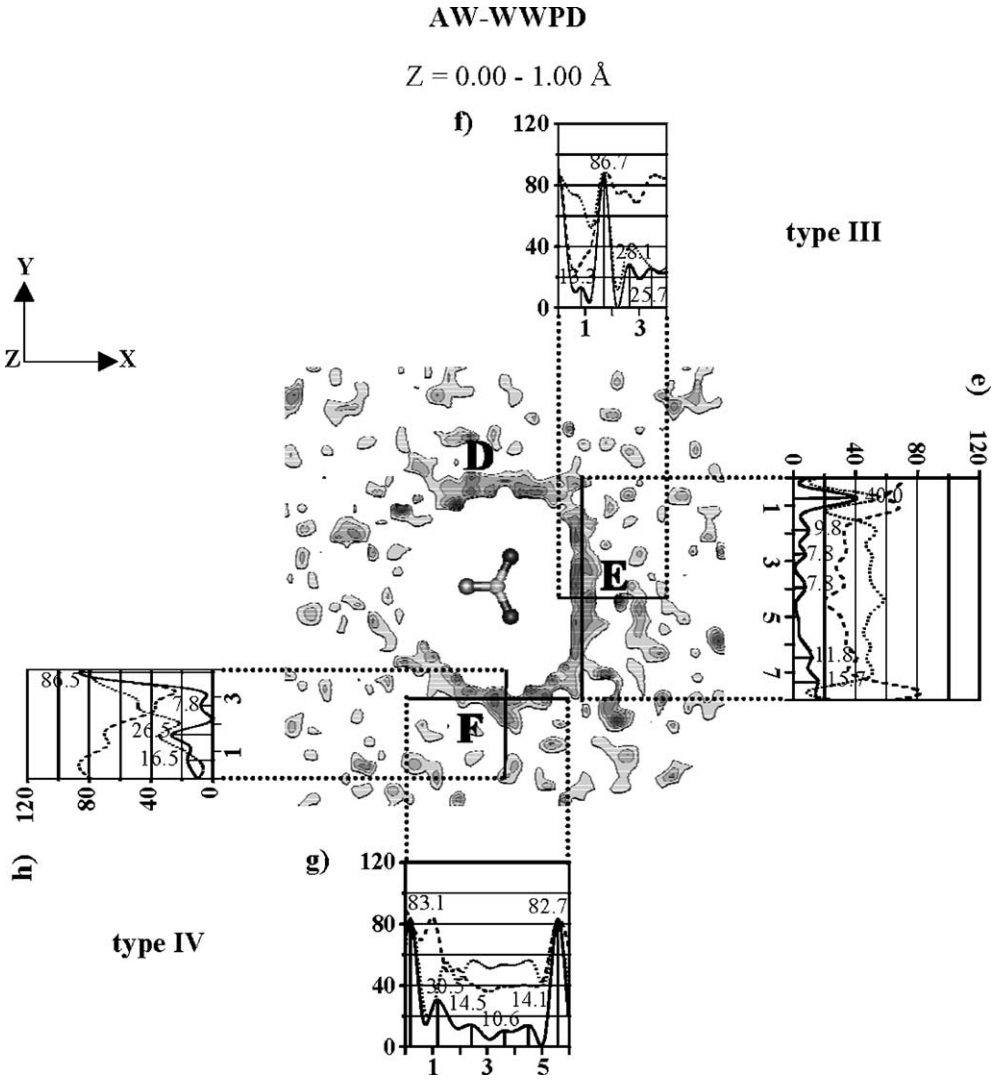

Fig. 5 (*continued*).

the H-bond network type **IV**$\langle E_{aq}^{L} \rangle$ inside the H-bond network type **III** in Fig. 5e are on average smaller than those inside the H-bond network type **IV** in Fig. 5g. However, the transverse AW-WWPD cross section plots in Fig. 5f and h suggest faster water exchange between the H-bond network type **IV** and the outsides, compared to that between the H-bond network type **III** and the outsides. This is in line with the values of $\tau_{\text{type IV, max}}$ and $\tau_{\text{type III, max}}$ of about 1 and 2 ps, respectively. Fig. 5e to h show that, in the vicinities of the highest contour densities of the H-bond network types **III** and **IV**, the AWPD cross section plots are lower than the WWPD cross section plots. They seem to define the shapes of the AW-WWPD cross section plots.

3.2.3. $[Gdm^{+}–FmO^{-}]_{aq}$

Selected results of MD-$[Gdm^{+}–FmO^{-}]^{R=3.9}_{aq,\ frozen}$ and MD-$[Gdm^{+}–FmO^{-}]^{R=3.9}_{aq,\ free}$ are displayed in Fig. 6, whereas those of MD-$[Gdm^{+}–FmO^{-}]^{R=6.3}_{aq,\ frozen}$ are illustrated in Fig. 7. The MD results showed that the close-contact $Gdm^{+}FmO^{-}$ complex is associated in aqueous solutions at 298 K, and $g(R)$ related to the hydration of the ion-pair complex, obtained from MD-$[Gdm^{+}–FmO^{-}]^{R=3.9}_{aq,\ free}$ and MD-$[Gdm^{+}–FmO^{-}]^{R=3.9}_{aq,\ frozen}$, are virtually the same. Therefore, only selected $g(R)$ deduced from MD-$[Gdm^{+}–FmO^{-}]^{R=3.9}_{aq,\ free}$ are displayed and discussed in details. This suggests further that the hydration structures obtained from these two MD conditions are similar and one could ascribe the three-dimensional structures of the H-bond networks of water for the freed close-contact ion-pair complex from MD-$[Gdm^{+}–FmO^{-}]^{R=3.9}_{aq,\ frozen}$.

Due to the symmetry of the close-contact $Gdm^{+}–FmO^{-}$ complex, the N2 and N3 atoms of Gdm^{+}, as well as the O1 and O2 atoms of FmO^{-}, are equivalent. $g(R)$ illustrated in Fig. 6a are related to the association of the close-contact $Gdm^{+}–FmO^{-}$ complex, whereas those in Fig. 6b to its hydration. The primary evidence for the association of the close-contact $Gdm^{+}–FmO^{-}$ complex in aqueous solutions obtained from $g(R_{C\cdots C})$ and $g(R_{N\cdots O})$ in Fig. 6a; all of which show single sharp peaks at the positions corresponding to the close-contact $Gdm^{+}–FmO^{-}$ complex in the gas phase. The main peak of $g(R_{C\cdots C})$ at R_{max} = 3.97 Å and those of $g(R_{N\cdots O})$

at R_{max} between 2.78 and 2.84 Å agree well with structure (a) in Fig. 3. The N–H···O H-bond distances are in line with the results obtained from high-resolution protein structural analyses of the Arg–COO^- complexes; the majority is within 2.6 and 3.0 Å [6]. The existence of $g(R_{N2\cdots O1})$, $g(R_{N2\cdots O2})$, $g(R_{N3\cdots O1})$ and $g(R_{N3\cdots O2})$ reflects the possibility for the H-bond donor–acceptor interchange between N2–H4···O1 and N3–H5···O2 H-bonds, by rotation of Gdm^+ and FmO^- about the C–N1 and C–H axes, respectively.

The formation of the close-contact Gdm^+ and FmO^- complex seems to block large part of the H-bond donor and acceptor functional groups, leading to remarkable changes in $g(R)$. As a consequence of the reduction of the H-bond network type **I**, the small peak of $g(R_{C\cdots Ow})$ at R_{max}=3.43 Å in $[Gdm^+]_{aq}$ becomes a shoulder in Fig. 6b. For MD-$[Gdm^+–FmO^-]^{R=3.9}_{aq,\ free}$, the main peaks of $g(R_{N2\cdots Ow})$, $g(R_{H\cdots Ow})$ and $g(R_{O1\cdots Ow})$ in Fig. 6b are smaller and broader, compared to those in $[Gdm^+]_{aq}$ and $[FmO^-]_{aq}$, respectively. Since the N1–H1 and N1–H2 groups are not directly involved in the ion-pair formation, $g(R_{N1\cdots Ow})$ is not substantially changed. In comparison with $[Gdm^+]_{aq}$, the position of the main peak of $g(R_{N1\cdots Ow})$ shifts slightly to longer distance, with a slight increase in the number of water molecules in close-contact with the N1–H1 and N1–H2 groups. The close-contact Gdm^+–FmO^- complex formation also reduces the possibility to form the H-bond network type **III**. In comparison to $[FmO^-]_{aq}$, the size of main peak of $g(R_{O\cdots Ow})$ is considerably reduced, accompanied by a reduction of the number of water molecules in close-contact with the COO^- group, from about two (1.8) to about one (1.3).

The three-dimensional structures of the H-bond networks of water in the first hydration shell of the close-contact Gdm^+–FmO^- complex, derived from MD-$[Gdm^+–FmO^-]^{R=3.9}_{aq,\ frozen}$, are displayed in Fig. 6c to e. It appears that the H-bond networks at **A** and **D**, as well as **B** and **F**, are quite associated and well-connected. Both of them seem to help stabilize of the close-contact Gdm^+–FmO^- complex in aqueous solutions. The H-bond networks linking between the Gdm^+ and FmO^- ions will be regarded as the H-bond network type **V**, see Fig. 6j and k. It seems that, within the H-bond network type **V**, water molecules could move or exchange in a wide range. $\tau_{type\ V,\ max}$ is only about 1 ps.

Fig. 6f to k show in general that the WWPD cross section plots are lower than the AWPD cross section plots, and the structures of the AW-WWPD cross section plots are determined by the structures of the WWPD cross section plots. This suggests that the net stabilization effect of the close-contact ion-pair complex arises partly from the H-bond networks caging around it. Similar conclusion was made based on calorimetric investigations on the binding affinities of the Gdm^+ derivatives and tetrabutylammonium acetate (TBA·AcO^-) in DMSO [55,56]. Under the experimental conditions in Ref. [55], it was concluded that the H-

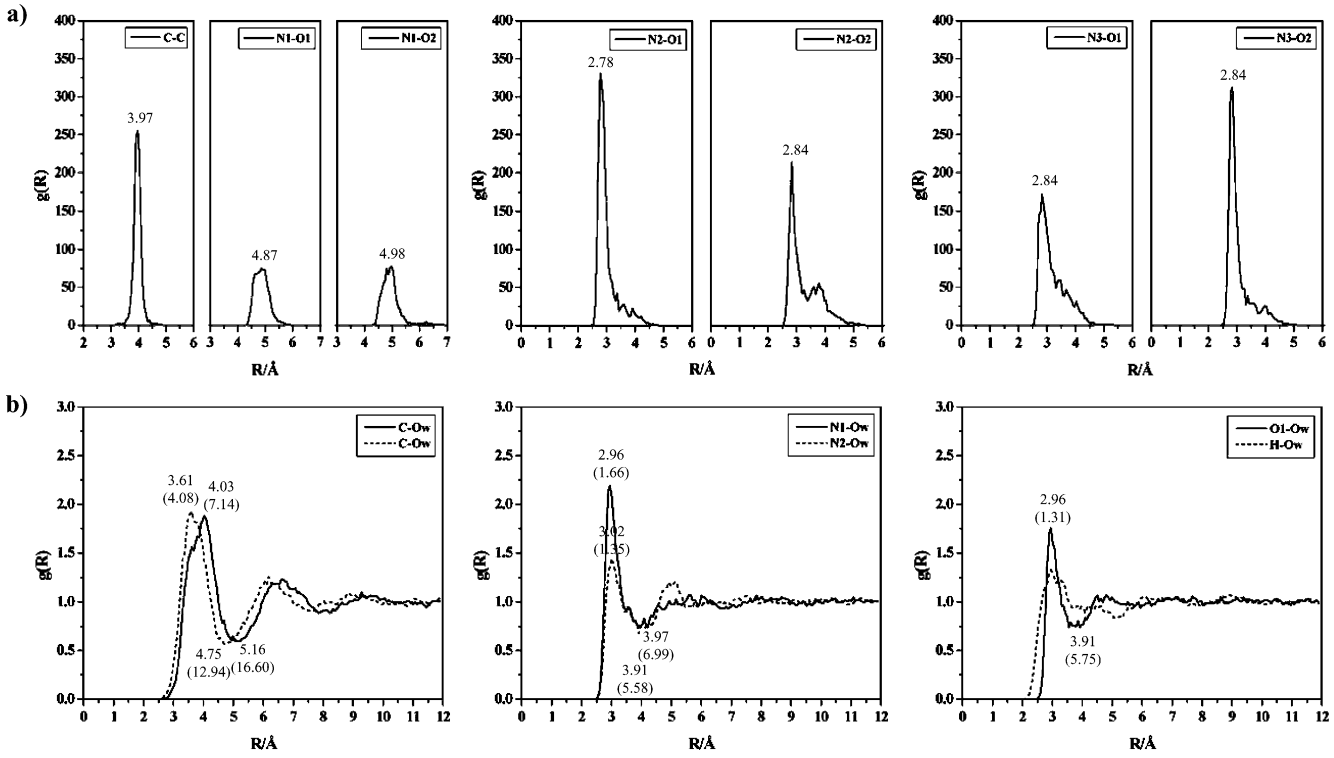

Fig. 6. Selected structure and energetic results obtained from MD-$[Gdm^+–FmO^-]^{R=3.9}_{aq,\ frozen}$ and MD-$[Gdm^+–FmO^-]^{R=3.9}_{aq,\ free}$. (a–b) $g(R)$ obtained from MD-$[Gdm^+–FmO^-]^{R=3.9}_{aq,\ free}$; characteristic distances are given, with $n(R)$ in parentheses. (c–e) The PDO, AWPD and AW-WWPD maps computed from MD-$[Gdm^+–FmO^-]^{R=3.9}_{aq,\ frozen}$. (f–k) Cross section plots computed from MD-$[Gdm^+–FmO^-]^{R=3.9}_{aq,\ frozen}$. —: The AW-WWPD cross section plot. ----: The AWPD cross section plot. ·····: The WWPD cross section plot. *X*-, *Y*- and *Z*-axes are in Å; energies are in kJ/mol.

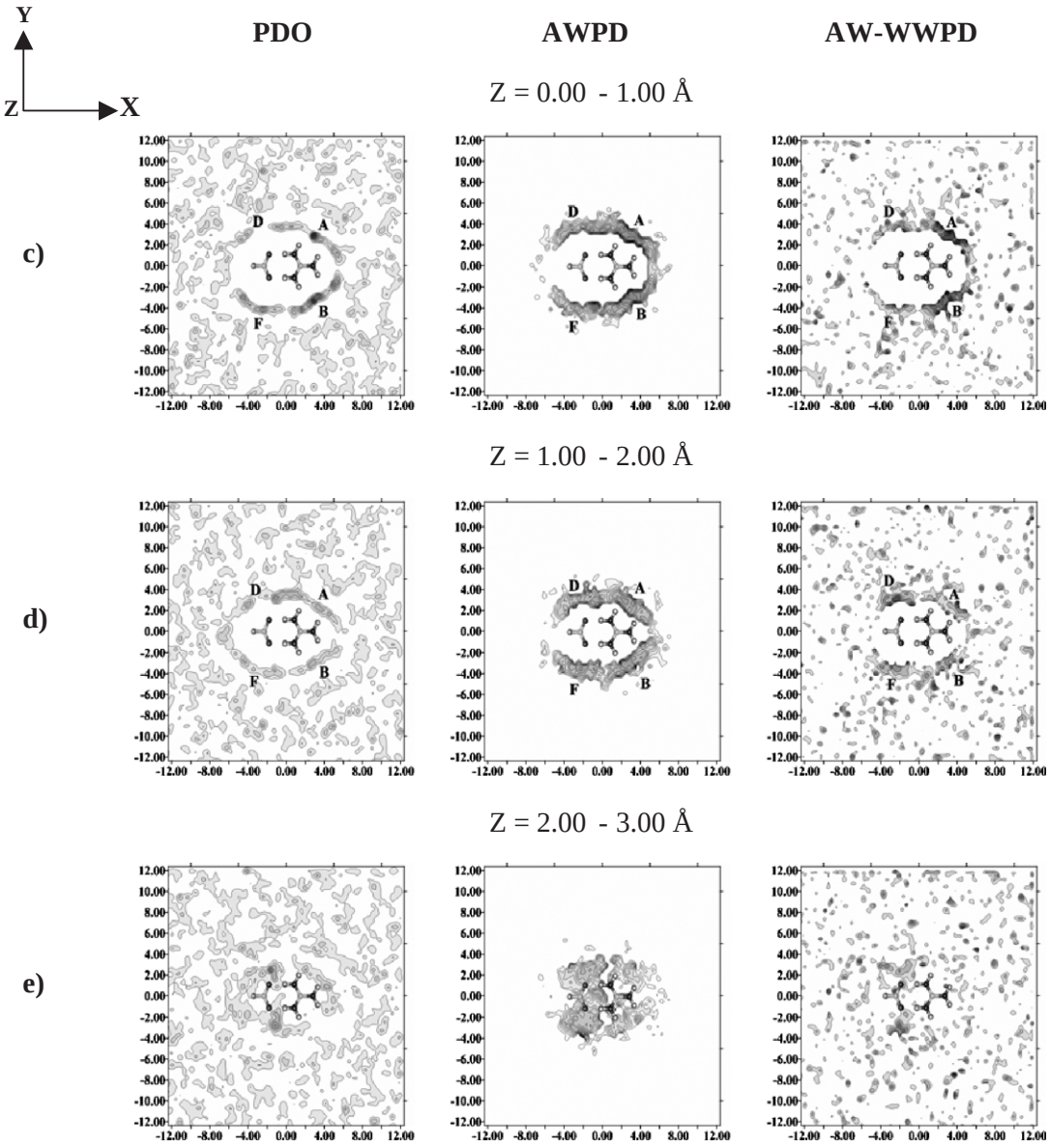

Fig. 6 (*continued*).

bonds between the Gdm^+ and COO^- ions seems not enough to direct ion-pair formation, and the affinities between the substrates and receptors are facilitated by solvent reorganization. The same explanation was put forward in Ref. [57], in which the solvent reactive field was pointed out to be the main reason for the association of pairs of monovalent ions over a wide range of interionic distances.

The close-contact Gdm^+–FmO^- complex formation leads to considerable changes in the structures of the longitudinal AW-WWPD cross section plot of the H-bond network type **I**, see Fig. 6f. The transition energy barriers to water exchange within the H-bond network type **I** ($\langle E_{aq}^{L} \rangle$) are increased, compared to $[Gdm^+]_{aq}$; whereas the transition energy barrier to water exchange between the H-bond network type **I** and the outsides($\langle E_{aq}^{T} \rangle$) is decreased to about 86 kJ/mol, see Fig. 6g. As a consequence, $\tau_{type\ I,\ max}$ is reduced to 6.9 ps, see Table 2 for comparison. The transverse AW-WWPD cross section plot in Fig. 6i also shows a decrease in the transition energy barrier to the water exchange between the H-bond network type **II** and the outsides; while the longitudinal AW-WWPD cross section plot is not much different. This leads to a decrease of $\tau_{type\ II,\ max}$ to about 7 ps.

The formation of the interstitial H-bond network of water between the Gdm^+ and FmO^- ions brings about changes in the structures and energetic of the H-bond network types **I**, **II** and **V**. The results from MD-$[Gdm^+–FmO^-]_{aq,\ frozen}^{R=6.3}$ in Fig. 7a and b illustrated that water molecules in the interstitial H-bond network, regarded as the H-bond network type **VI**, are very localized, especially in the layer with $Z=1–2$ Å. The longitudinal and transverse WWPD cross section plots in Fig. 7h and i clearly show that the H-bonds between water molecules in the H-bond network type **VI** are very weak, as a consequence of strong H-bond interactions between the water molecules and the solute ions. The difference between

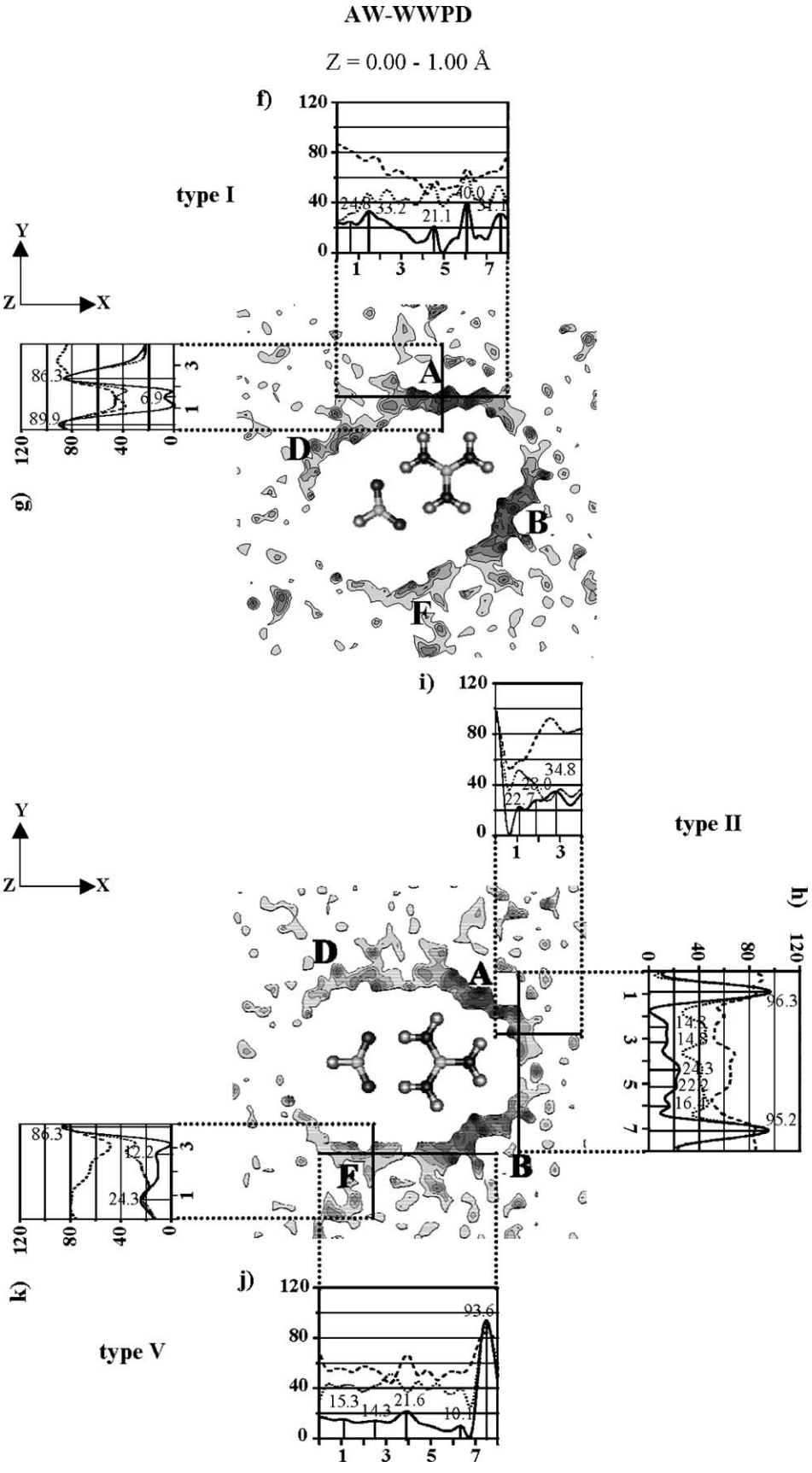

Fig. 6 (*continued*).

the solute–solvent and solvent–solvent interaction energies amounts approximately to 100 kJ/mol, see Fig. 7h. In the interstitial H-bond network, the mobility of water molecules is rather restricted, only within a small and narrow energy valley of about 2 Å width, see Fig. 7h and i. This is in accordance with $\tau_{\text{type VI, max}}$ of about 18 ps. The shapes of the transverse and longitudinal AW-WWPD cross section plots of the H-bond network types **I** and **II**, obtained from MD-$[Gdm^+–FmO^-]^{R=6.3}_{aq,\ frozen}$, resemble those from MD-$[Gdm^+]_{aq}$; whereas the H-bond network type **V** seems to be less connected compared to MD-$[Gdm^+–FmO^-]^{R=3.9}_{aq,\ frozen}$.

Under the present MD simulations conditions, the solvent-separated $Gdm^+–FmO^-$ complex seems not favorable in aqueous solutions. When all molecules were allowed to move in MD-$[Gdm^+–FmO^-]^{R=6.3}_{aq,\ free}$, $g(R_{C\cdots C})$ and $g(R_{N\cdots O})$, not shown here, revealed that the solvent-separated $Gdm^+–FmO^-$ complex was disrupted, due mainly to strong solute–solvent and weak solvent–solvent H-bond interactions within the interstitial H-bond network. This is different from the results of the PMF calculations [13,14,36], in which the second minimum, corresponding to the solvent-separated ion-pairs, was observed on the free energy profiles at the interionic distances approximately between 6 and 7 Å. A plausible explanation for the discrepancy was given in details in Refs. [13,58], in which an artifact of the relative orientation constraint imposed in the PMF calculations was pointed out to be one of the main reasons. The applicability and short-

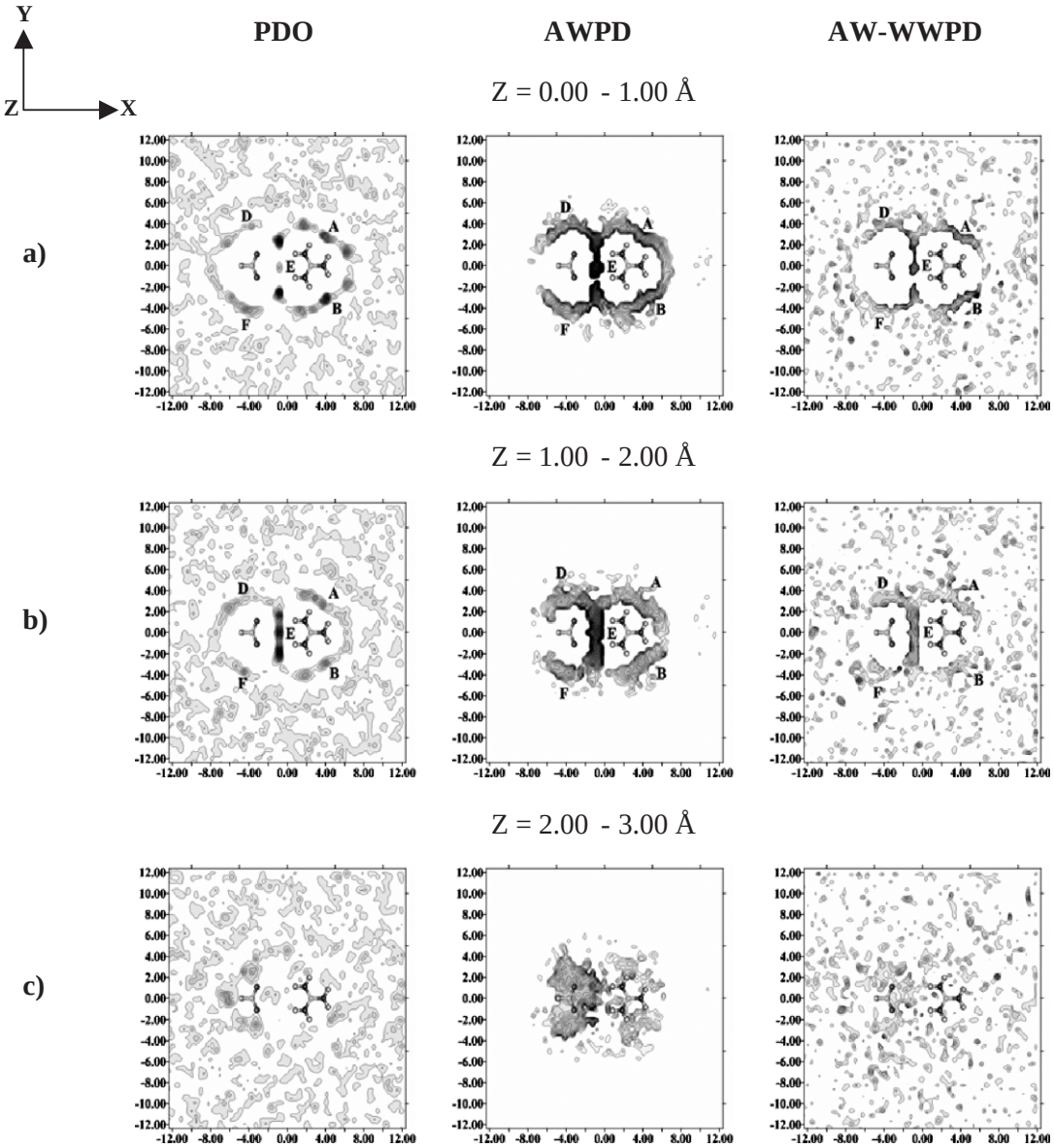

Fig. 7. Selected structure and energetic results obtained from MD-$[Gdm^+$-$FmO^-]^{R=6.3}_{aq,\ frozen}$. (a–c) The PDO, AWPD and AW-WWPD maps. (d–k) Cross section plots. —: The AW-WWPD cross section plot. ----: The AWPD cross section plot. ·····: the WWPD cross section plot. *X*-, *Y*- and *Z*-axes are in Å; energies are in kJ/mol.

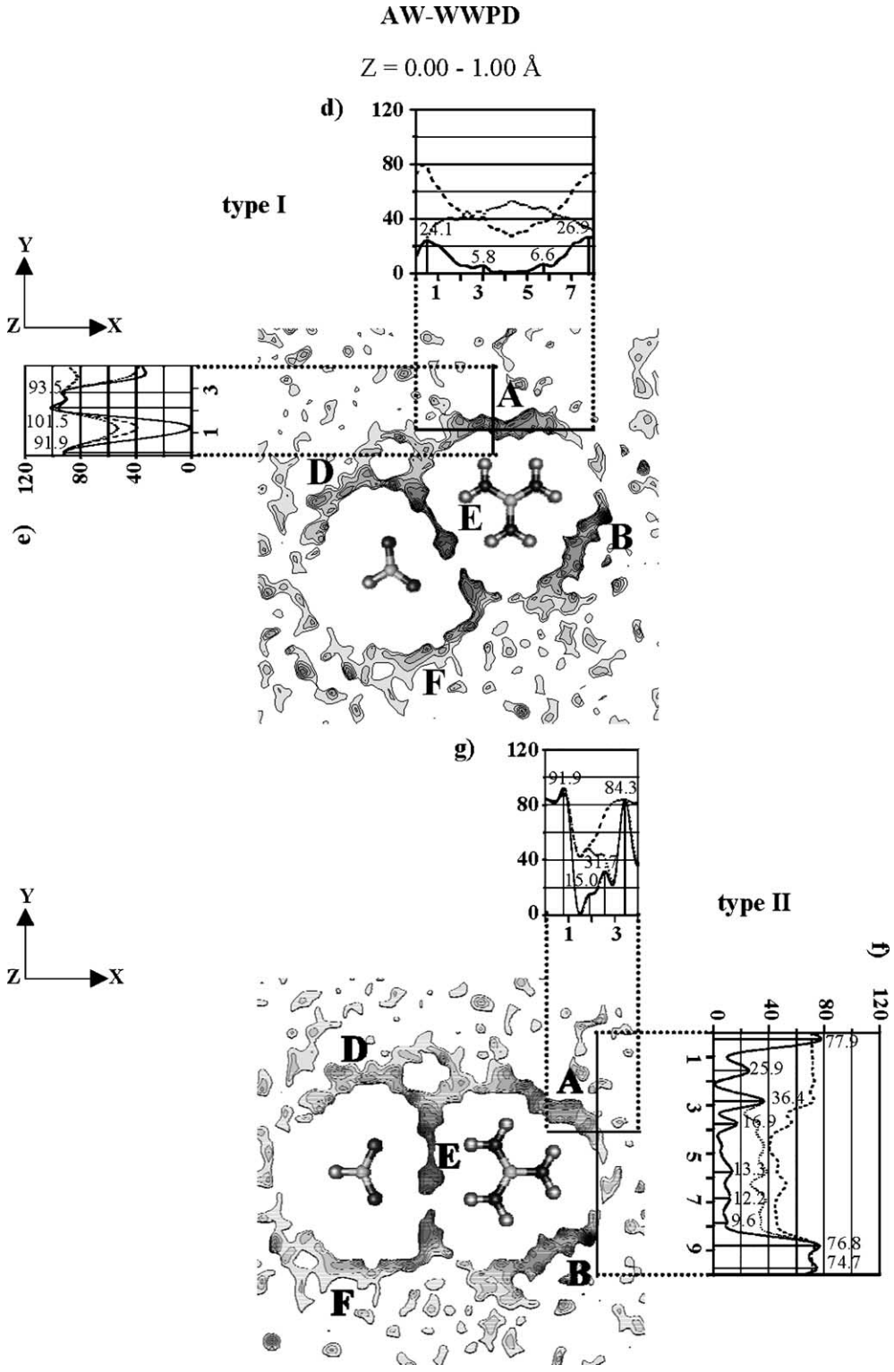

Fig. 7 (*continued*).

comings of theoretical methods for free energy calculations have been addressed in details in Refs. [59,60] and will not be repeated here.

It should be mentioned that the theoretical results reported in the present work are based on a pair-wise additive scheme, in which the many-body or polarization effects are not included in the model calculations. Based on MD simulations on $[NaCl]_{aq}$, with polarizable and nonpolarizable water models, the dependence of some ionic-solution properties on the polarizability was found to

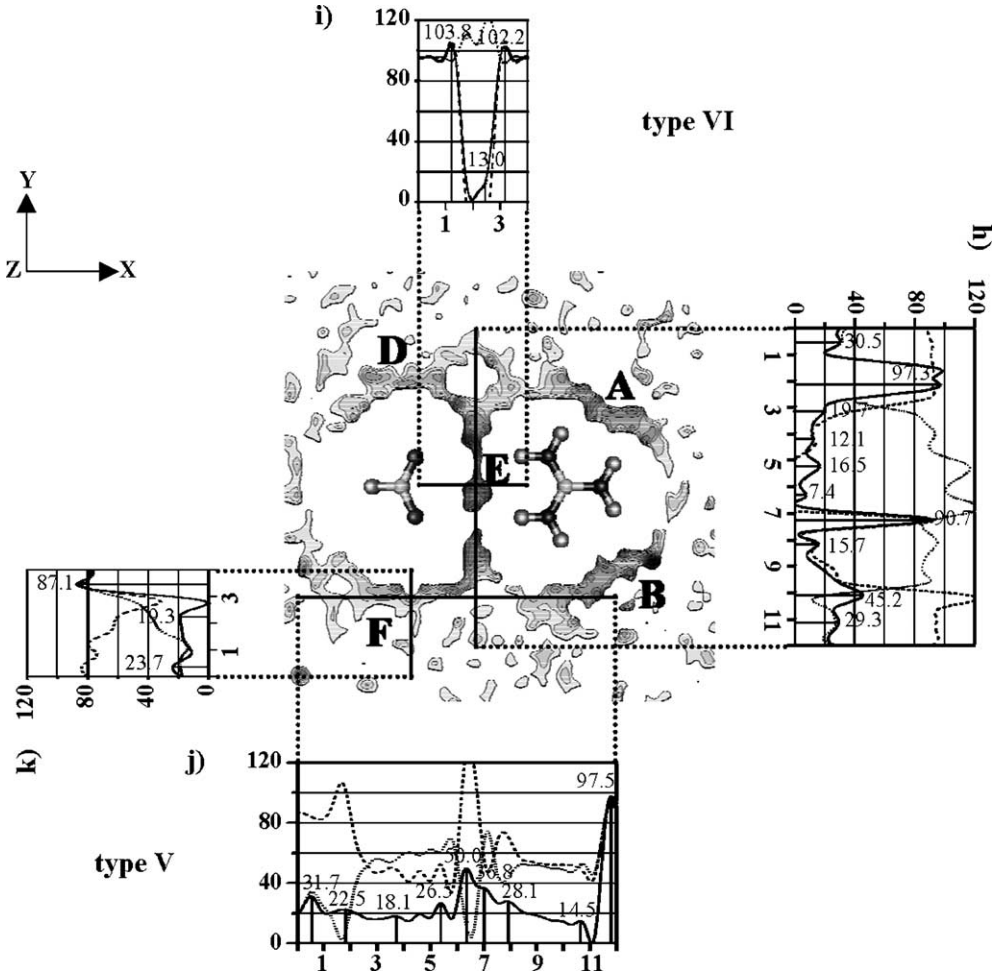

Fig. 7 (*continued*).

be moderate [42], with slightly larger effects at the highly polarizable Cl^- ion. Since the ions and the ion-pair considered in the present work are considerably larger than monovalent ions, the polarization effects could be expected to be smaller; due to lower charge densities on atoms. Additionally, it was reported in Ref. [57] that, when polarization effects were introduced to a model calculation, the ion clusters exhibited less structure, with lower degree of ionic hydrations; due to the destabilization of the solute–solvent interactions in the first hydration shell. Since a destabilization of the solute–solvent interactions is usually accompanied by a stabilization of the solvent–solvent interactions [21], and our MD results suggested that the associations of water molecules in the first hydration shell are partly responsible for the net stabilization of the close-contact ion-pair, we anticipate that the close-contact ion-pair will become more associated if polarization effects are included in our model calculation. The results on the solvent-separated ion-pair are also expected to remain the same, due to the fact that the solute–solvent interactions in the interstitial H-bond network are considerably stronger than the solvent–solvent interactions.

4. Conclusion

Structures and stability of salt-bridge in aqueous solution were studied using a complex formed from the guanidinium (Gdm^+) and formate (FmO^-) ions as a model system. The theoretical investigations were started with construction of intermolecular potentials to describe the interactions in $[Gdm^+]_{aq}$, $[FmO^-]_{aq}$ and $[Gdm^+–FmO^-]_{aq}$, using the T-model. The T-model potentials were tested in the calculations of equilibrium structures and interaction energies of the $Gdm^+–H_2O$, $FmO^-–H_2O$ and $Gdm^+–FmO^-$ 1:1 complexes in the gas phase. The lowest-lying minimum energy geometries of these 1:1 complexes were examined using ab initio calculations at MP2 levels of theory. It appeared that, cyclic-bifurcated H-bond complexes represent the most stable structures in the gas phase. The structural and energetic results obtained from the T-model potentials agreed well with ab initio calculations at the MP2 levels.

Based on the computed T-model potentials, the three-dimensional structures and energetic of the H-bond networks of water in the first hydration shell of the Gdm^+ and FmO^- ions, as well as the $Gdm^+–FmO^-$ complex, were investigated, by conducting series of MD simulations. The

PDO maps obtained from the analyses of MD results suggested two types of the H-bond networks in the first hydration shell of $[Gdm^+]_{aq}$, regarded as the H-bond network types **I** and **II** in the present study. Both of them are located on the Gdm^+ molecular plane and seem to be quite well-connected. The analyses of the cross section plots revealed that the solute–solvent interactions dominate the solvent–solvent interactions for the H-bond network type **I**, whereas the situation is opposite for the H-bond network type **II**. The structures of the average potential energy landscapes in $[Gdm^+]_{aq}$ suggested further that water molecules inside the H-bond network type **I** should have higher mobility compare to the H-bond network type **II**.

Due to the fact that the FmO^- ion is a strong proton acceptor, the three-dimensional structures and energetic of the H-bond networks in the first hydration in $[FmO^-]_{aq}$ are different from $[Gdm^+]_{aq}$. The PDO maps showed that the H-bond network at the COO^- group is located slightly above the FmO^- plane; the longitudinal cross section plots revealed that water molecules could move or exchange in a wider range, especially in the H-bond network type **III**. The detail structures of the longitudinal and transverse cross section plots suggested that, near the energy minima in the H-bond network types **III** and **IV**, the solute–solvent interactions dominate the solvent–solvent interactions.

The MD results on $[Gdm^+–FmO^-]_{aq}$ revealed that the close-contact ion-pair formation leads to considerable changes in the hydration structures and energetic of the aqueous solutions. In the first hydration shell, the longitudinal and transverse cross section plots indicated stronger solvent–solvent H-bond interactions compared to the solute–solvent H-bond interactions. This suggested that water molecules in the first hydration shell form solvent cages around the ion-pair complex, leading to a net stabilization effect to the close-contact ion-pair complex. Similar conclusions were put forward in the cases of $[Gdm^+\text{-}TBA{\cdot}AcO^-]_{DMSO}$ and the aqueous solutions of ion-pairs formed from monovalent ions. The solvent reorganization and solvent reactive field were pointed out to be responsible for the ion-pair associations in the solutions, respectively. Due to strong solute–solvent and weak solvent–solvent H-bond interactions in the interstitial H-bond network, the present MD simulations predicted that the solvent-separated $Gdm^+–FmO^-$ complex are disrupted in aqueous solutions.

Attempt has been made in the present work to account for the dynamic behavior of water molecules in the first hydration shell of solutes, using the structures of the average potential energy landscapes and the longest H-bond lifetime defined in our previous investigation. Although the average potential energy landscapes in $[Gdm^+]_{aq}$, $[FmO^-]_{aq}$ and $[Gdm^+–FmO^-]_{aq}$ are rather complicated and irregular, the computed longest H-bond lifetimes are reasonable, compared with the residence times obtained from other MD simulations and NMR experiments. The longest H-bond lifetime could be associated with the water molecule which takes the rate-determining water exchange path, by assuming that the water molecule with the longest H-bond lifetime enters the first hydration shell by taking the path with the highest transition energy barriers. The longest H-bond lifetime, therefore, represents a simple and reasonable alternative to introduce the dynamic behavior of water molecules in definition of the first hydration shell; a specific water molecule is considered to reside in the first hydration shell of solute only when it is trapped long enough in it.

Finally, it should be mentioned that the present theoretical results were based on a pair-wise additive scheme, in which the many-body or polarization effects were not included in the model calculations. However, based on the MD simulations on ion-pairs of monovalent ions in aqueous solutions, and the fact that the ions and ion-pairs considered here possess lower charge densities on atoms, compared to the monovalent ions, it is reasonable to believe that the present results will not be substantially changed if cooperative effects are included in the model calculations.

Acknowledgement

All calculations were performed at the School of Chemistry, Suranaree University of Technology. Supaporn Chaiyapongs would like to acknowledge the financial support from the Commission on Higher Education (CHE) and Ramkhamhaeng University (RU). This work was supported in part by the ASEA-UNINET and the University of Innsbruck, Austria.

References

[1] D. Gandini, L. Gogioso, M. Bolognesi, D. Bordo, Pattern of ionizable sidechains interactions in protein structures, Proteins: Struct., Funct., Genet. 24 (1996) 439–449.
[2] D.J. Barlow, J.M. Thornton, Ion-pairs in proteins, J. Mol. Biol. 168 (1983) 867–885.
[3] J.F. Riordan, K.D. McElvany, C.L. Borders Jr., Arginyl residues: anion recognition sites in enzymes, Science 195 (1977) 884–886.
[4] J.F. Kirsch, G. Eichcle, G.C. Ford, M.G. Vincent, J.N. Jansonius, H. Gehring, P. Christen, Mechanism of action of aspartate aminotransferase proposed on the basis of its spatial structure, J. Mol. Biol. 174 (1984) 497–525.
[5] J. Tormo, D. Blaas, N.R. Parry, D. Rowlands, D. Stuart, I. Fita, Crystal structure of a human rhinovirus neutralizing antibody complexed with a peptide derived from viral capsid protein VP2, EMBO J. 13 (1994) 2247–2256.
[6] J. Singh, J.M. Thornton, M. Snarey, S.F. Campbell, The geometries of interacting arginine-carboxyls in proteins, FEBS Lett. 224 (1987) 161–171.
[7] M.P. Fülscher, E.L. Mehler, Ab initio interaction potentials of guanidine-formic acid in neutral and charged states, J. Mol. Struct., Theochem 165 (1988) 319–327.
[8] Y.-J. Zheng, R.L. Ornstein, What happens to salt-bridges in non-aqueous environments: insights from quantum mechanics calculations, J. Am. Chem. Soc. 118 (1996) 11237–11243.

[9] X. Barril, C. Alemán, M. Orozco, F.J. Luque, Salt bridge interactions: stability of the ionic and neutral complexes in the gas phase, in solution, and in proteins, Proteins: Struct., Funct., Genet. 32 (1998) 67–79.
[10] A. Melo, M.J. Ramos, W.B. Floriano, J.A.N.F. Gomes, J.F.R. Leão, A.L. Magalhães, B. Maigret, M.C. Nascimento, N. Reuter, Theoretical study of arginine–carboxylate interactions, J. Mol. Struct., Theochem 463 (1999) 81–90.
[11] J.B.O. Mitchell, J.M. Thornton, J. Singh, S.L. Price, Towards an understanding of the arginine–aspartate interaction, J. Mol. Biol. 226 (1992) 251–262.
[12] J.A. Ippolito, R.S. Alexander, D.W. Christainson, Hydrogen bond stereochemistry in protein structure and function, J. Mol. Biol. 215 (1990) 457–471.
[13] S. Saigal, J. Pranata, Monte Carlo simulations of guanidinium acetate and methylammonium acetate ion pairs in water, Bioorg. Chem. 25 (1997) 11–21.
[14] X. Rozanska, C. Chipot, Modeling ion–ion interaction in proteins: a molecular dynamics free energy calculation of the guanidinium–acetate association, J. Chem. Phys. 112 (2000) 9691–9694.
[15] T.A. Keith, M.J. Frisch, in: D.A. Smith (Ed.), Inclusion of Explicit Solvent Molecules in a Self-Consistent-Reaction Field Model of Solvation, Modeling the Hydrogen Bond, ACS Symposium Series, vol. 569, American Chemical Society, Washington, 1994, p. 22.
[16] K. Sagarik, S. Dokmaisrijan, A theoretical study on hydration of alanine zwitterions, J. Mol. Struct., Theochem 718 (2005) 31–47.
[17] H.J. Böhm, R. Ahlrichs, A study of short-range repulsions, J. Chem. Phys. 77 (1982) 2028–2034.
[18] J. Hoinkis, R. Ahlrichs, H.J. Böhm, A simple treatment of intermolecular interactions: synthesis of ab initio calculations and combination rules, Int. J. Quant. Chem. 23 (1983) 821–834.
[19] H.J. Böhm, R. Ahlrichs, P. Scharf, H. Schiffer, Intermolecular potentials for CH_4, CH_3F, CHF_3, CH_3Cl, CH_2Cl_2, CH_3CN and CO_2, J. Chem. Phys. 81 (1984) 1389–1395.
[20] H.J. Böhm, R. Ahlrichs, Molecular dynamics simulation of liquid CH_2Cl_2 and $CHCl_3$ with new pair potentials, Mol. Phys. 54 (1985) 1261–1274.
[21] E. Clementi, Computational aspects for large chemical systems, Lecture Notes in Chemistry, vol. 19, Springer-Verlag, Berlin, 1980.
[22] K.P. Sagarik, R. Ahlrichs, Molecular dynamics simulations of liquid $CHClF_2$ with a test-particle model potential, Chem. Phys. Lett. 131 (1986) 74–81.
[23] K.P. Sagarik, R. Ahlrichs, S. Brode, Intermolecular potentials for ammonia based on the test particle model and the coupled pair functional method, Mol. Phys. 57 (1986) 1247–1264.
[24] K.P. Sagarik, R. Ahlrichs, A test particle model potential for formamide and molecular dynamics simulations of the liquid, J. Chem. Phys. 86 (1987) 5117–5126.
[25] K.P. Sagarik, V. Pongpituk, S. Chaiyapongs, P. Sisot, Test-particle model potentials for hydrogen-bonded complexes: complexes formed from HCN, HF, H_2O, NH_3, $HCONH_2$, $HCONHCH_3$, guanine and cytosine, Chem. Phys. 156 (1991) 439–456.
[26] K. Sagarik, E. Spohr, Statistical mechanical simulations on properties of liquid pyridine, Chem. Phys. 199 (1995) 73–82.
[27] K. Sagarik, P. Asawakun, Intermolecular potential for phenol based on the test particle model, Chem. Phys. 219 (1997) 173–191.
[28] K. Sagarik, Theoretical studies on hydrogen bonding in hydroxylamine clusters and liquid, J. Mol. Struct., Theochem 465 (1999) 141–155.
[29] K. Sagarik, B.M. Rode, Intermolecular potential for benzoic acid–water based on the test-particle model and statistical mechanical simulations of benzoic acid in aqueous solutions, Chem. Phys. 260 (2000) 159–182.
[30] K. Sagarik, S. Chaiwongwattana, P. Sisot, A theoretical study on clusters of benzoic acid–water in benzene solutions, Chem. Phys. 306 (2004) 1–12.
[31] C.M. Breneman, K.B. Wiberg, Determining atom-centered monopoles from molecular electrostatic potentials. The need for high sampling density in formamide conformational analysis, J. Comput. Chem. 11 (1990) 361–373.
[32] M.J. Frisch, G.W. Trucks, H.B. Schlegel, G.E. Scuseria, M.A. Robb, J.R. Cheeseman, V.G. Zakrzewski, J.A. Montgomery, R.E. Stratmann, J.C. Burant, S. Dapprich, J.M. Millam, A.D. Daniels, K.N. Kudin, M.C. Strain, O. Farkas, J. Tomasi, V. Barone, M. Cossi, R. Cammi, B. Mennucci, C. Pomelli, C. Adamo, S. Clifford, J. Ochterski, G.A. Petersson, P.Y. Ayala, Q. Cui, K. Morokuma, D.K. Malick, A.D. Rabuck, K. Raghavachari, J.B. Foresman, J. Cioslowski, J.V. Ortiz, B.B. Stefanov, G. Lui, A. Liashenko, P. Piskorz, I. Komaromi, R. Gomperts, R.L. Martin, D.J. Fox, T. Keith, M.A. Al-Laham, C.Y. Peng, A. Nanayakkara, C. Gonzalez, M. Challacombe, P.M.W. Gill, B.G. Johnson, W. Chen, M.W. Wong, J.L. Andres, M. Head-Gordon, E.S. Replogle, J.A. Pople, Gaussian, vol. 98, Gaussian Inc., Pittsburgh, 1998.
[33] P.L. Cummins, J.E. Gready, The electrostatic potential in the semi-empirical molecular orbital approximation, Chem. Phys. Lett. 225 (1994) 11–17.
[34] S.F. Boys, F. Bernardi, The calculation of small molecular interactions by the differences of separate total energies. Some procedures with reduced errors, Mol. Phys. 19 (1970) 553–566.
[35] Y. Su, E. Gallicchio, The non-polar solvent potential of mean force for the dimerization of alanine dipeptide: the role of solute–solvent van der Waals interactions, Biophys. Chem. 109 (2004) 251–260.
[36] K. Sagarik, S. Chaiyapongs, Structures and stability of model salt-bridge interaction in aqueous solution, Proceedings of the 8th Annual National Symposium on Computational Science and Engineering (ANSCSE-8), Suranaree University of Technology, Nakhon Ratchasima, Thailand, 2004, p. 9.
[37] SURFER for Window, Version 6.04, Golden Software Inc., USA, 1997.
[38] K. Wüthrich, in: K. Wüthrich (Ed.), Hydration of Biological Macromolecules in Solution: Surface Structure and Molecular Recognition, NMR in Structural Biology, World Scientific Series in 20th Century Chemistry, vol. 5, World Scientific, Singapore, 1995, p. 647.
[39] M. Odelius, A. Laaksonen, in: P.B. Balbuena, J.M. Seminario (Eds.), Combined MD Simulation–NMR Relaxation Studies of Molecular Motion and Intermolecular Interactions, Molecular Dynamics from Classical to Quantum Methods, Theoretical and Computational Chemistry, vol. 7, Elsevier, Amsterdam, 1999, p. 281.
[40] R.M. Brunne, E. Liepinsh, G. Otting, K. Wüthrich, W.F. van Gunsteren, Hydration of proteins: a comparison of experimental residence times of water molecules solvating the bovine pancreatic trypsin inhibitor with theoretical model calculations, J. Mol. Biol. 231 (1993) 1040–1048.
[41] R.W. Impey, P.A. Madden, I.R. McDonald, Hydration and mobility of ions in solution, J. Phys. Chem. 87 (1983) 5071–5083.
[42] D.E. Smith, L.X. Dang, Computer simulations of NaCl association in polarizable water, J. Chem. Phys. 100 (1994) 3757–3766.
[43] D.A. Case, D.A. Pearlman, J.W. Caldwell, T.E. Cheatham III, W.S. Ross, C. Simmerling, T. Darden, K.M. Merz, R.V. Stanton, A. Cheng, J.J. Vincent, M. Crowley, V. Tsui, R. Radmer, Y. Duan, J. Pitera, I. Massova, G.L. Seibel, U.C. Singh, P. Weiner, P.A. Kollman, AMBER, Version 6, University of California, San Francisco, 1999.
[44] W.L. Jorgensen, J. Tirado-Rives, The OPLS potential functions for proteins. Energy minimizations for crystals of cyclic peptides and crambin, J. Am. Chem. Soc. 110 (1988) 1657–1666.
[45] J. Gao, in: D.A. Smith (Ed.), Computation of Intermolecular Interactions with a Combined Quantum Mechanical and Classical Approach, Modeling the Hydrogen Bond, ACS Symposium Series, vol. 569, American Chemical Society, Washington, 1994, p. 8.
[46] M.J. Field, P.A. Bash, M. Karplus, A combined quantum mechanical and molecular mechanical potential for molecular dynamics simulations, J. Comput. Chem. 11 (1990) 700–733.

[47] I. Lukovits, A. Karpfen, H. Lischka, P. Schuster, Ab initio LCMO studies on the hydration of formate ion, Chem. Phys. Lett. 63 (1979) 151–154.
[48] W.L. Jorgensen, J. Gao, Monte Carlo simulations of the hydration of ammonium and carboxylate ions, J. Phys. Chem. 90 (1986) 2174–2182.
[49] J. Gao, D.S. Garner, W.L. Jorgensen, Ab initio study of structures and binding energies for anion–water complexes, J. Am. Chem. Soc. 108 (1986) 4784–4790.
[50] F.J. Luque, N. Reuter, A. Cartier, M.F. Ruiz-López, Calibration of the quantum/classical Hamiltonian in semiempirical QM/MM AM1 and PM3 methods, J. Phys. Chem., A 104 (2000) 10923–10931.
[51] L. Shimoni, J.P. Glusker, C.W. Bock, Energies and geometries of isographic hydrogen-bonded networks: 1. The $R_2^2(8)$ graph set, J. Phys. Chem. 100 (1996) 2957–2967.
[52] H.G. Hertz, in: F. Franks (Ed.), Water, A Comprehensive Treatise, vol. 3, Plenum Press, New York, 1973.
[53] F. Brugè, E. Parisi, S.L. Fornili, Effects of simple model solutes on water dynamics: residence time analysis, Chem. Phys. Lett. 250 (1996) 443–449.
[54] I. Muegge, E.W. Knapp, Residence times and lateral diffusion of water at protein surfaces: application to BPTI, J. Phys. Chem. 99 (1995) 1371–1374.
[55] B. Linton, A.D. Hamilton, Calorimetric investigation of guanidinium–carboxylate interactions, Tetrahedron 55 (1999) 6027–6038.
[56] E. Fan, S.A. Van Arman, S. Kincaid, A.D. Hamilton, Molecular recognition: hydrogen-bonding receptors that function in highly competitive solvents, J. Am. Chem. Soc. 115 (1993) 369–370.
[57] D. Laria, R. Fernández-Prini, Molecular dynamics study of water clusters containing ion pairs: from contact to dissociation, J. Chem. Phys. 102 (1995) 7664–7673.
[58] C. Chipot, B. Maigret, D.A. Pearlman, P.A. Kollman, Molecular dynamics potential of mean force calculations: a study of the toluene–ammonium π–cation interactions, J. Am. Chem. Soc. 118 (1996) 2998–3005.
[59] P. Kollman, Free energy calculations: applications to chemical and biological phenomena, Chem. Rev. 93 (1993) 2395–2417.
[60] A.R. Leach, Molecular Modelling: Principles and Applications, Longman, Singapore, 1996.